JGP Journal of General Physiology

TUTORIAL

Analysis methods and quality criteria for investigating muscle physiology using x-ray diffraction

John M. Squire[1,2] and Carlo Knupp[3]

X-ray diffraction studies of muscle have been tremendously powerful in providing fundamental insights into the structures of, for example, the myosin and actin filaments in a variety of muscles and the physiology of the cross-bridge mechanism during the contractile cycle. However, interpretation of x-ray diffraction patterns is far from trivial, and if modeling of the observed diffraction intensities is required it needs to be performed carefully with full knowledge of the possible pitfalls. Here, we discuss (1) how x-ray diffraction can be used as a tool to monitor various specific muscle properties and (2) how to get the most out of the rest of the observed muscle x-ray diffraction patterns by modeling where the reliability of the modeling conclusions can be objectively tested. In other x-ray diffraction methods, such as protein crystallography, the reliability of every step of the process is estimated and quoted in published papers. In this way, the quality of the structure determination can be properly assessed. To be honest with ourselves in the muscle field, we need to do as near to the same as we can, within the limitations of the techniques that we are using. We discuss how this can be done. We also use test cases to reveal the dos and don'ts of using x-ray diffraction to study muscle physiology.

Introduction

In the early 1950s, the first examinations of muscle structures by x-ray diffraction were being performed (e.g., Huxley, 1953). At around the same time, x-ray diffraction studies from protein crystals were initiated, and the technique of protein crystallography was established (Perutz, 1949). For muscle and with protein crystals, usually a thin monochromatic x-ray beam is used to illuminate the specimen, and on the other side of the specimen, a diffraction pattern can be recorded (Fig. 1 a). As described by Squire (Squire, 1981, 2019), these methods are examples of imaging techniques. In the case of microscopes (optical or electron), the beams diffracted or scattered into the objective lens are refocused onto a point in the image plane, and an image of the scattering object can be formed. All of the scattered beams (each having wave properties) are associated with an intensity (brightness) and a relative phase. Recombining the scattered beams with the correct amplitude (square root of intensity) and phase produces the required image. Light and electron lenses preserve the relative phases of the scattered beams along their path through the instrument so that a good image is produced. However, x-ray beams are not easily focused, so all that can be done is to record the diffraction pattern on a film or detector to obtain the distribution of diffracted intensities. Unfortunately, this process removes knowledge of the phases associated with each beam, so half of the information needed to produce an image is missing. This is known as the phase problem. In protein crystallography, x rays are typically directed onto a single crystal that is rotated to different angles in the x-ray beam, and a pattern is recorded for each angle. A full set of 3-D diffraction information is obtained. In the mid- to late 1900s, protein crystallography methods were developed to obtain indirect experimental estimates of the phases, thus enabling an image to be obtained in a computer using all the known amplitudes and phases. The method is enormously powerful and, with suitable crystals, can solve structures to very high resolutions and with objectively assessed reliability (Wlodawer et al., 2008).

Diffraction from muscle is intrinsically different from diffraction from a single crystal. In striated muscles, the sarcomeres are within myofibrils that have random rotations around the muscle fiber axis. Myofibrils are parts of fibers that also have random rotations. This means that diffraction patterns recorded

[1]Muscle Contraction Group, School of Physiology, Pharmacology and Neuroscience, University of Bristol, Bristol, UK; [2]Faculty of Medicine, Imperial College, London, UK; [3]School of Optometry and Vision Sciences, Cardiff University, Cardiff, UK.

John M. Squire died on January 31, 2021; Correspondence to Carlo Knupp: knuppc@cardiff.ac.uk

This work is part of a special collection on myofilament function and disease.

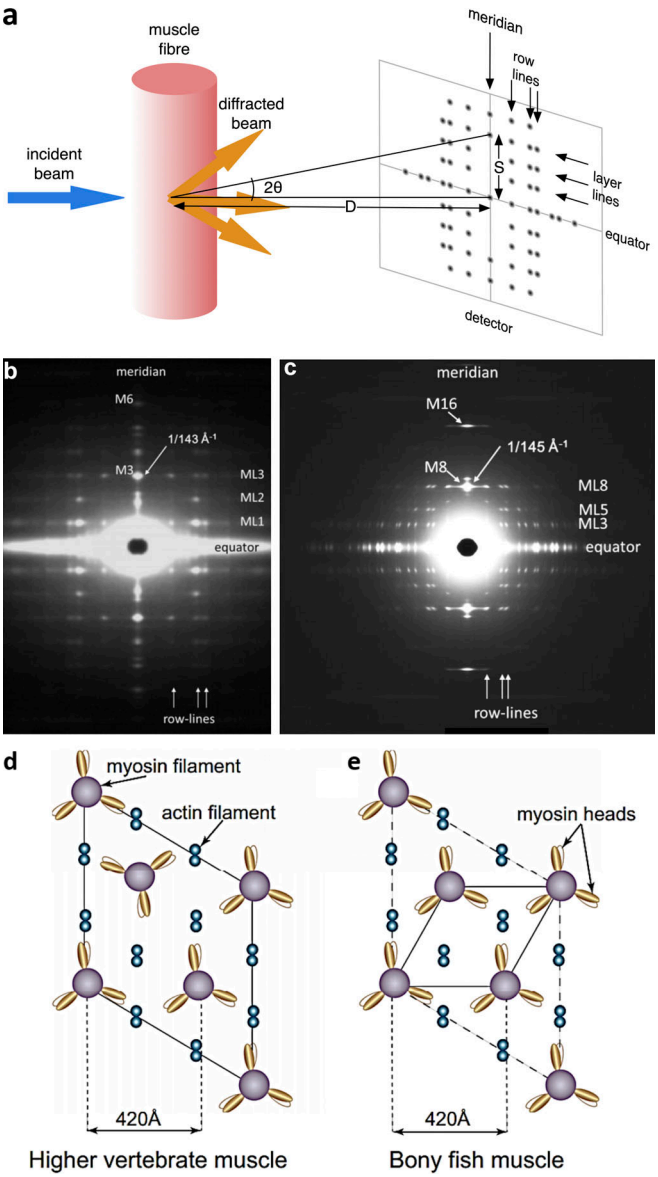

Figure 1. **Schematic diagram of the geometry of a fiber x-ray diffraction pattern. (a)** A narrow, monochromatic beam of x rays entering from the left impinges on the (vertical) fiber, which diffracts the x rays onto a screen or detector. Typical fiber diffraction patterns consist of a symmetrical pattern of horizontal lines of intensity known as "layer lines," with the layer line through the pattern center known as the equator. The central vertical axis is the meridian. The axial positions of the layer lines (S) tell us about the axial periodicities of the diffracting objects in the fiber, provided the x-ray wavelength (λ) and the camera length (D) are known. The angle of diffraction (2θ) is $\tan^{-1}$ (S/D). This can be put into Bragg's law ($n\lambda = 2\,d \sin\theta$) to calculate the value of d, the spacing in the diffracting object. Bragg's law shows that the larger d is, the smaller is 2θ; there is a reciprocal relationship between the spacings in diffracting objects and the positions of the diffraction spots that they give rise to. The middle of a diffraction pattern provides low-resolution information, and the resolution increases as spots occur farther away from the center. For fibers that are well ordered in 3-D, the horizontal layer lines will be broken up into spots of intensity that lie along vertical row lines. In diffraction patterns from well-ordered muscles, the equator and layer lines are all sampled on the same row lines, which provide information about the lattice of filaments in the muscle, particularly the A-band. Less well-ordered muscles may have sampling along the equator, but not along the layer lines. Fig. 1 a is reproduced from Squire and Knupp (2017). **(b)** Low-angle x-ray diffraction pattern from bony fish muscle in the relaxed state (Harford and Squire, 1986). Meridional peaks are labeled M3, M6, and so forth, and myosin layer lines are labeled ML1, ML2, and so forth. For details, see text. **(c)** Low-angle x-ray diffraction pattern from insect flight muscle in the relaxed state (courtesy of Prof. Mike Reedy, Duke University, Durham, NC). Labeling is similar to b. **(d)** The A-band lattice in higher-vertebrate fast muscles such as those in frog sartorius showing different rotations of the myosin filaments around their long axes, producing a superlattice structure (Huxley and Brown, 1967; Luther and Squire, 1980, 2014). **(e)** The equivalent lattice to d but for simple lattice muscles such as bony fish muscle, where all the myosin filaments have exactly the same rotations forming a regular, quasi-crystalline A-band (Harford and Squire, 1986; Luther and Squire, 1980). The quoted lattice dimensions are approximate; there is variation between muscles and with sarcomere length. Fig. 1, d and e, is modified from Luther and Squire (1980).

from muscle are patterns obtained from diffraction information that is rotated around the fiber axis; many of the intensities are smeared together. This is a so-called cylindrically averaged diffraction pattern, known as a "fiber diffraction pattern" (it also applies to many other kinds of fiber apart from muscle; see Fraser and MacRae, 1973). In this case, as well as having the phase problem to deal with, different diffracted beams overlap and are difficult to unscramble.

There are very few good methods to find the phases in fiber diffraction patterns. A different approach is needed. What can be done is to make an informed guess at a possible model structure, calculate its expected diffraction pattern, and compare this with what is observed. If the fit is not good enough, the model can be adjusted to make the agreement better. However, there is as yet no generally agreed method of assessing the validity of models obtained from x-ray fiber diffraction data from muscle. It is sometimes the case that very different models will fit the observed diffraction patterns equally well. Here, we discuss this problem in more detail and outline a possible objective quality control method by which to know whether any models that are produced can be relied on. We also show how x-ray diffraction from muscle in some cases can be used as a tool to determine various muscle features in a relatively unambiguous way without modeling.

There are several papers and books on the x-ray fiber diffraction technique available in the literature (e.g., Holmes and Blow, 1965; Vainshtein, 1966; Fraser and MacRae, 1973; Chandrasekaran and Stubbs, 2012) and several reviews on the application of fiber diffraction methods to muscle (Squire, 1981; Harford and Squire, 1997; Squire, 2000; Squire and Knupp, 2005, 2017; Squire, 2019). The present paper does not revisit these fundamental principles; the interested reader should look at some of these older reviews. Here we add to those reviews in discussion of (1) how to use x-ray diffraction as a tool to determine various muscle properties and (2) how to model x-ray diffraction data from muscle with a sensible measure of reliability.

Description of muscle x-ray diffraction patterns

Despite the problem with fiber diffraction studies, muscle is a relatively kind specimen in that many striated muscles are well enough ordered to give beautifully rich diffraction patterns. Examples are given in Fig. 1, b and c. Most muscle x-ray diffraction

patterns have the same basic appearance. With the fiber axis vertical, the diffracted intensity falls along horizontal layer lines, with the layer line through the center of the pattern being called the "equator" (Fig. 1, a–c). Myosin filaments and actin filaments are all quasi-helical structures, and they give their own characteristic layer-line patterns (Squire, 1981). In vertebrate muscles and other muscles such as those from tarantula, the axial repeats in the actin and myosin filaments are different, meaning that their layer lines fall at different axial positions and can be separated. Insect flight muscle is different in the sense that the actin and myosin filaments have related axial repeats and some of their layer lines overlap (AL-Khayat et al., 2003). The central vertical line in the diffraction pattern is the meridian, and actin and myosin filaments both contribute to this, as well as other sarcomere components such as C-protein and troponin (Offer et al., 1973; Rome et al., 1973a, 1973b; Bordas et al., 1993; Martin-Fernandez et al., 1994; Squire et al., 2017).

The equator of the x-ray diffraction pattern, the horizontal line through the pattern center (Fig. 1 a), arises from the density distribution through the muscle sarcomere when viewed down the fiber axis. This means that the actin and myosin filaments, with all their associated proteins, contribute to what is seen on the equator. Muscles with regular A-bands, such as vertebrate striated and insect flight muscles, show well-defined diffraction peaks along the equator that arise from the hexagonal lattice of filaments present in the muscle A-bands. Other muscles with less well-ordered lattices give equatorial intensity that may be only partially sampled. In 3-D, if the myosin and actin filaments do not have regular rotations around their long axes, then the sampling seen along the equator is not repeated in the layer lines, which may be partially sampled (if there is a superlattice; Fig. 1 d) or completely unsampled, depending on the degree of order in the muscle. However, some striated muscles such as bony fish muscle and insect flight muscle are such that all the myosin filaments have the same rotation around their long axes right across the A-band. They are what is known as "simple lattice muscles" (Harford and Squire, 1986; Luther and Squire, 1980, 2014; see Fig. 1 e for bony fish muscle; a simple lattice has also been seen in vertebrate slow muscle; Ma et al., 2019). The result of this is that all the layer lines are sampled in the same way as the equator (Fig. 1, b and c). In the case of bony fish muscle, the myosin filaments are on a simple lattice, and the myosin layer lines are sampled as on the equator, giving vertical row lines of intensity (Fig. 1, b and c), but the actin filaments are not as well organized, and the actin layer lines are relatively unsampled. In insect flight muscle, however (Reedy, 1968; AL-Khayat et al., 2003; Perz-Edwards et al., 2011), the myosin and actin filaments are both well organized, so all the layer lines, including those from actin, are well sampled on row lines out to a certain resolution (Fig. 1 c).

Setting up models

As we discuss later, parts of the muscle diffraction pattern can be used as tools to directly detect or measure various sarcomere features, but other parts of the pattern, including much of the meridian, are not easily interpreted, and in such cases it is often necessary to set up models for the various muscle components in terms of variable parameters that can be changed until there is good agreement between the observed and calculated diffraction patterns. Such models are heavily dependent on what we know already about various components of muscle. One of the good things about x-ray fiber diffraction is that the positions of the diffraction spots can be measured, often quite accurately, and these give direct, unambiguous information about the spacings and dimensions of objects in the fiber, from which the filament symmetry can often be deduced (see Squire, 1981). The lattice spacing (lateral filament separation) can be determined directly from the equatorial spacings, and this is a help in monitoring what is happening to the lattice, such as the sarcomere length changes, or as a consequence of myosin head binding to actin in active muscle, or in skinned fibers that have swelled during the preparation process. The axial spacings of the layer lines can, for example, define the axial repeats in the myosin and actin filaments. From the equator, we can find the size of the A-band lattice unit cell. The use of layer line peak positions can also be used as a measure of the mean radial position of the heads.

If modeling is required, we now know the structures of the myosin head in various states (Rayment et al., 1993; Dominguez et al., 1998; Houdusse and Sweeney, 2016; Sweeney et al., 2020) and of G-actin (Kabsch et al., 1990). From high-resolution EM and single-particle analysis, we now have good structures for the whole thin filament with tropomyosin and myosin head labeling (Behrmann et al., 2012; von der Ecken et al., 2016) and evidence about the location of troponin (Paul et al., 2017; Yamada et al., 2020). There are also good structures for the myosin filaments from a variety of muscles (e.g., Woodhead et al., 2005; Zoghbi et al., 2008; AL-Khayat et al., 2008, 2013; Hu et al., 2016; Daneshparvar et al., 2020). In the case of human cardiac muscle myosin filaments, there are suggestions about the locations of titin (Brynnel et al., 2018) and myosin-binding protein-C (Offer et al., 1973; AL-Khayat et al., 2013). The all-important questions, then, are about how proteins such as the myosin head, C-protein, tropomyosin, and troponin move when muscle contracts. In other words, how does muscle work? Time-resolved x-ray fiber diffraction is a very powerful method to study some of these things. Here we discuss methods to achieve the most reliable results about the physiology of the contractile mechanism.

Assessment of the quality of models

The necessity to have quality criteria associated with conclusions from modeling muscle properties using x-ray diffraction data are obvious; without them, it may well be that totally false conclusions are reached that others will take as fact.

In an abstract way, we can think of a model as a set of functions that can be used, given some parameter values, to calculate the expected values of the observations. Let us assume that we have a set of observations O_1, O_2, O_3, ... O_N. The model can be thought of as a set of functions F_1, F_2, ... F_N, dependent on the parameters P_1, P_2, P_3, and so forth that can be used to calculate the expected values of O. The complexity of the model will be mirrored by the complexity of the functions representing it. Finding the correct values for the model parameter is therefore equivalent to solving the system of simultaneous equations:

$$F_1(P_1, P_2, P_3, \ldots) = O_1$$
$$F_2(P_1, P_2, P_3, \ldots) = O_2$$
$$F_3(P_1, P_2, P_3, \ldots) = O_3$$
$$F_N(P_1, P_2, P_3, \ldots) = O_N$$

The question is, how many model parameters P can be determined uniquely given a set of observations O? The answer clearly depends on the model; that is, on the functions F_1, F_2, ... F_N. In a best-case scenario, the functions are a linear combination of the parameter values P_1, P_2, and so forth. In this case, the minimum number of observations needed to determine the parameter values is the same as the number of parameters used. Any fewer observations, and the parameters are not uniquely determined; we might find parameters that fit the observations, but there will be many other possible solutions. But this is a best-case scenario. The functions F_1, F_2, ... F_N could be a higher-degree combination of the parameters P_1, P_2, P_3, and so forth. In this case, the number of observations needed to determine the values of the parameters could be much higher, depending on the complexity of the model. In light of this, it is easy to see how important it is to keep the models simple and make sure that there are enough observations to fit them. At the very least, if the number of observations is smaller than the number of parameters needed to define the model, it is very unlikely that the model parameters can be uniquely determined.

Also, with muscle diffraction data, the experimental observations are subject to experimental errors; to be happy with any modeling that is performed, it is much healthier to make sure that the number of observations is significantly greater than the number of parameters to be determined.

Estimating the number of independent observations

The estimation of the number of truly independent observations being used for modeling depends on the kind of diffraction pattern that is being studied and the predicting power of the models themselves (essentially the form of the particular set of equations F_1, F_2, ... mentioned above). If the pattern is one of the discrete spots along layer lines, as in the case of those from bony fish muscle (Fig. 1 b) and insect flight muscle (Fig. 1 c), and assuming the lattice dimensions have been defined, then the simplest models will make specific predictions for the intensity of each spot of the diffraction pattern. Therefore, each spot in one quadrant can be taken as one observation, as can each meridional peak. There may be additional information to use, if appropriate, such as the peak widths, which give an idea of the extent of the diffracting array and the degree of order in the lattice, but these need to be estimated considering several diffraction peaks together, and the number of extra observations will not be large (Eakins et al., 2019).

In the case of continuous layer lines where the intensity varies smoothly with the radius from the meridian, sampling the intensity along the layer line more finely in an attempt to increase the number of observations is not a recommended strategy, because this could only be supported meaningfully by prohibitively complex models. A good way to think about the number of independent observations in a smooth curve, which in turns sets the constraint for the complexity of the models that can be tested, is to estimate how well the curve could be fitted by, say, a polynomial function or a set of overlapping Gaussian shapes or a Bessel function and then to estimate how many parameters are needed to generate the polynomial, the Gaussians, or the Bessel function. In the simplest case, the observed peak shape may approximate just to a single Gaussian, and, for the kind of simple models usually used in the muscle field, even though the intensity might have been sampled in, say, 100 positions along the layer line, the shape only needs three parameters to fit it, namely the position of the Gaussian center along the layer line, the width of the Gaussian, and its peak height (or, alternatively, its area). More complex profiles might require more Gaussians to fit them, and the effective number of observations will increase accordingly.

Note that another way to proceed could be to use the equatorial peaks, if the equator is sampled, to show where row lines would have been if the muscle had been "crystalline" and the layer lines had been sampled as well. However, any modeling should not then assume that the object is a crystal. This approach is saying that the structure to be modeled in the muscle is bounded by the edges of the unit cell defined by the equatorials. In doing the modeling, the diffracting object must still be considered to be cylindrically averaged and the diffraction pattern unsampled.

Take as an example the intensity profile along the actin sixth layer line at 59 Å in Fig. 2 a (green trace). This is from bony fish muscle set at a sarcomere length of 2.2 µm and in the relaxed state (Eakins et al., 2018). It is not a simple Gaussian shape, so Eakins et al. have used PeakFit (http://sigmaplot.co.uk/products/peakfit/peakfit.php) to try to reproduce it as a sum of Gaussians. Fig. 2 c shows that to fit the whole profile across the meridian of the diffraction pattern reasonably well requires only five Gaussians. One of these is the peak on the meridian. The others occur in symmetrical pairs that can be averaged across the meridian, so only three independent Gaussians are needed to fit the whole profile. This gives width and peak height for the meridian and position, width, and peak height for the two peaks describing the off-meridional part of the intensity, eight observations in all. It would be fair to say that to fit this 59 Å layer line with a model, even though the intensity may be sampled at 100 points, contributes only eight independent observations. With several actin layer lines, the number of independent observations can build up, but it is still necessary to check that the total number of free parameters in any model that is being tested is less than the number of observations.

As described later, there are objective ways of determining whether the use of extra model parameters is justified.

Test case 1: Modeling actin filaments

Another approach to modeling the thin filament was used by Squire et al. (1993) and Al-Khayat et al. (1995). The modeling of the actin filament in the relaxed and active states (in nonoverlap muscle to remove the complications of myosin head labeling) used features of the observed actin layer lines 1–8 with a model representation of the actin monomer as four spheres. The strands of tropomyosin were represented by overlapping spheres (Fig. 2 b). In principle, each sphere representing an actin subdomain

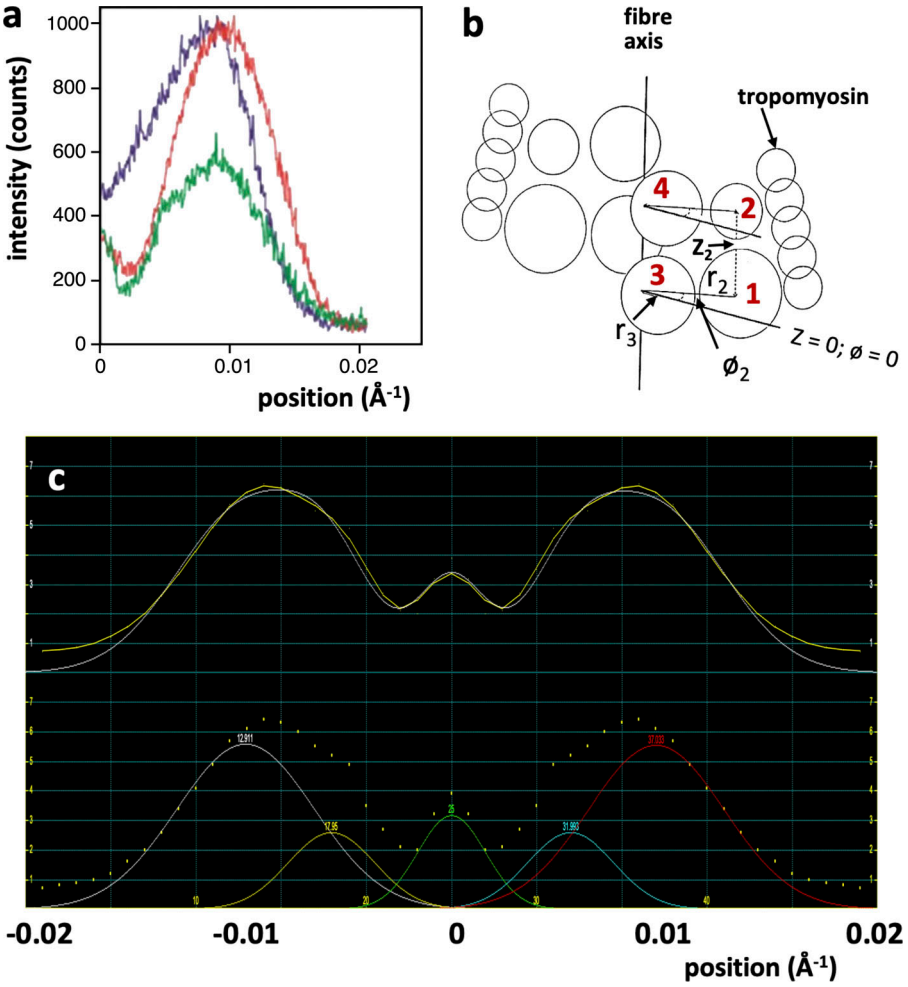

Figure 2. **Fitting x-ray reflections. (a)** Intensity profile along the sixth actin layer line at ~59 Å from bony fish muscle in three different states: resting muscle (green), rigor muscle at 2.2-µm sarcomere length (blue), and rigor muscle at 2.5-µm sarcomere length (red). Reproduced from Eakins et al. (2018). **(b)** The simple geometry needed to model actin/tropomyosin filament structure out to ~45 Å resolution: four spheres for actin, one for each subdomain, and a set of equal overlapping spheres for tropomyosin. The origin for measurement of the azimuthal angle (Ø) and the axial position Z was taken as the center of actin subdomain 3. For details, see text. Adapted from Al-Khayat et al., 1995. **(c)** Profile of the green trace in a showing both sides of the meridian (intensity vertical axis; position 0 is the meridian) and profile fitting by five overlapping Gaussian functions using PeakFit (http://sigmaplot.co.uk/products/peakfit/peakfit.php). For details, see text.

required its position to be defined by four parameters: the sphere radius (R), the radial position of the sphere center from the filament axis (r), an azimuthal angle (ø; rotation angle around the filament axis), and an axial position (z). There are four actin subdomains, so this would give 16 unknown parameters. We do know the relative weights of the subdomains, so the value of R could be calculated accordingly, assuming a uniform protein density. However, there is a need for a reference point in space, so the values of ø and z for one subdomain (subdomain 3 was chosen; Fig. 2 b) could be set to 0 and everything else defined relative to the position of that subdomain. This left 10 unknown parameters to be determined for the actin part of the thin filament. The tropomyosin strands, represented as overlapping spheres each of radius R_{TM} (once again determined by the weight of tropomyosin) and assumed to be on a perfect helix, required a radius from the helix axis (r_{TM}) and azimuth ($ø_{TM}$). The whole analysis therefore required the determination of 10 unknown parameters for actin and 2 for tropomyosin. The possible effects of disorder were not considered at this stage.

In this study, the defined task was to determine the low-resolution changes in thin-filament structure on going from the relaxed to the active state in nonoverlap muscle. As far as observations were concerned, the observed peak shapes along the layer lines in the two states were defined not as layer line profiles as in Fig. 2 a but in terms of a small range of radial positions for each observed peak and their intensity relative to that on the sixth layer line at 59 Å, which was taken as a reference. There were therefore 8 layer lines with 2 parameters from each for 2 filament states, giving 32 observations to be fitted. The 59 Å peak height from relaxed muscle used as a reference reduced this to 31. An additional observation was the known radius of gyration of the actin filament (Hartt and Mendelson, 1980).

The starting point of the calculations was a simulation of the F-actin structure determined by Holmes et al. (1990) and Lorenz et al. (1993). In addition, the positions of the actin subdomains were not considered to be totally free in that they were constrained within a given monomer to be within sensible proximity to each other; they are all part of the same protein molecule. This applied to the separations of covalently linked subdomains 1 and 2, 1 and 3, and 3 and 4. So, the effective number of free parameters was considerably less than 31. The results, which showed sensible movements of tropomyosin and particularly of subdomain 2 between the relaxed and active states, were therefore fully justified by the observations being fitted and the constraints on the modeling.

Note that the protein nebulin (Kiss et al., 2020), which is also present in some actin filaments, was not included in this

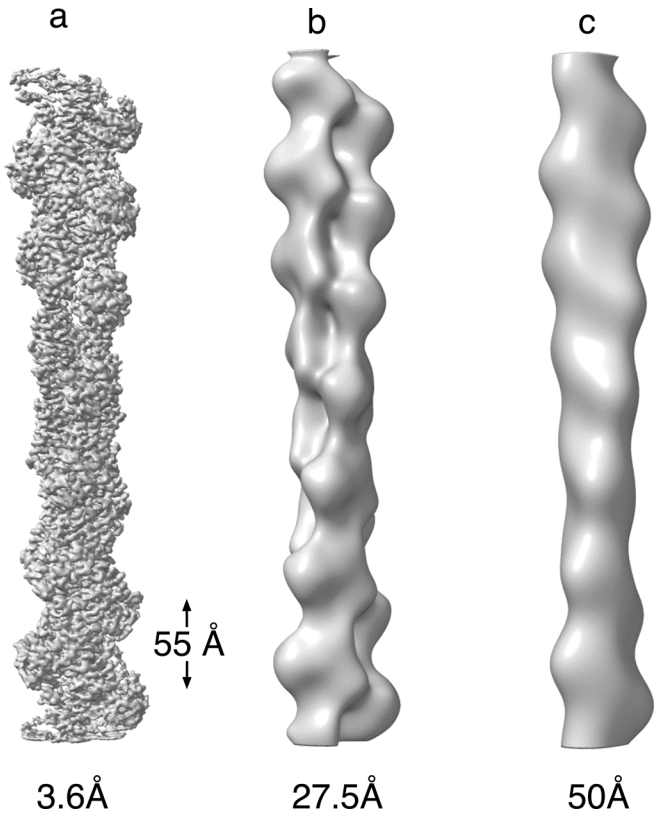

Figure 3. **Space-filling representations of F-actin filaments at three different resolutions. (a)** 3.6 Å resolution. **(b)** 27.5 Å resolution. **(c)** 50 Å resolution. Low-angle x-ray diffraction patterns from muscle actin usually show layer lines out to ∼51 Å resolution, sometimes out to the meridional reflection at 27.5 Å. Even at that higher resolution, the detail in the structure is not great. Modeling with the kind of simplified approximation in Fig. 2 b is quite justified. Courtesy of Danielle Paul and Marston Bradshaw.

modeling. Nebulin has a molecular weight per actin contractile unit (seven actins, one tropomyosin, and one troponin) of ∼32 kD compared with actin (∼7 × 42 = 294 kD), tropomyosin (∼70 kD), and troponin (∼80 kD). Were it to run along the tropomyosin strands, it would add ∼50% to the mass of tropomyosin. Remembering that intensity is a function of the square of the mass, it would add ∼25% to the tropomyosin diffraction contribution). The structure and role of nebulin in the thin filaments have yet to be determined, although they are known to be involved in thin filament length determination (Kiss et al., 2020). The tropomyosin contributes mainly to the lower-order actin layer lines (1–3), and very little to the 6th (59 Å) and 7th (51 Å) layer lines, so the omission of nebulin in the calculations would probably have had little effect on the conclusions.

Note that fitting data such as the low-angle diffraction patterns from actin filaments, as one usually obtains from intact muscle, does not need definition of the actin filament structure at high resolution. At best, muscle x-ray diffraction patterns show layer lines to ∼27.5 Å resolution, and often layer lines are recorded only to the sixth or seventh layer lines at 59 Å and 51 Å, respectively. Courtesy of Danielle Paul and Marston Bradshaw (School of Physiology, Pharmacology and Neuroscience, University of Bristol, Bristol, UK), Fig. 3 shows what the F-actin filament looks like when viewed at different resolutions; namely (a) 3.6 Å, (b) 27.5 Å, and (c) 59 Å. The whole high-resolution structure (a) could, of course, be used in modeling, but the usual problem is one of reducing computing time to manageable values. With many parameters, and doing global searches over those parameters, or even simulated annealing procedures (e.g., Hudson et al., 1997), estimated computing times can range from hours to years, so simplifying the problem in a sensible way makes it practically possible to reach good conclusions in realistic times. Having said that, it is possible when a conclusion has been reached using a sphere model to replace the final model by a suitably adjusted high-resolution structure and then to refine this structure against the observations, although this is not necessary and is not often done.

Representing the subdomains as spheres is quite adequate in solving low-angle x-ray diffraction data from actin filaments. In fact, Parry and Squire (1973) successfully modeled the actin filament and tropomyosin shift out to the seventh layer line just with single spheres for the whole actin monomer and overlapping spheres for the tropomyosin, and the results have stood the test of time (see also Huxley, 1973; Haselgrove, 1973; Vibert et al., 1997; Squire and Morris, 1998). With better data, the more detailed modeling of the actin monomer as four subdomains, as done by Squire et al. (1993) and Al-Khayat et al. (1995) (Fig. 2 b), was able to confirm the tropomyosin shift and also to show the significant movement of actin subdomain 2 without the need to go to higher resolution.

Test case 2: Modeling myosin filaments in relaxed "quasi-crystalline" muscles

Turning now to the modeling of the cross-bridge array and other components of the muscle myosin filament, the task is very much simplified if the muscle is well ordered as in relaxed bony fish muscle (Fig. 1 b) and insect flight muscle (Fig. 1 c). Here, each observed diffraction peak in one quadrant and on the meridian of the well-sampled diffraction patterns can be considered as an independent observation. There are four copies of each (two of the meridionals) because the four quadrants are, in principle, equivalent if the muscle is at 90° to the x-ray beam. These can be averaged to get a more reliable intensity figure for each peak. If the incident angle is not 90°, the pattern will appear asymmetric across the equator, but equivalent reflections in the four quadrants can still be combined if the pattern is converted to reciprocal space and then properly peak fitted (e.g., using FiberFix; Rajkumar et al., 2007).

Once the peak intensities have been determined, modeling then depends on how many parameters are needed to do the job properly. In the case of vertebrate muscle, there are three crowns of heads in a 430 Å repeat, with six heads in each crown. We know there are perturbations of the structure (Huxley and Brown, 1967; Harford and Squire, 1986; AL-Khayat et al., 2013), so the three crowns do not all have the same structure, even though their origins on the backbone may be along helical tracks (AL-Khayat et al., 2008). At a minimum, we need to find an R for the head origins in each the three crowns and then an azimuthal angle, an axial tilt, and an angle of rotation of each head around its long axis. Assuming that the filament array has threefold

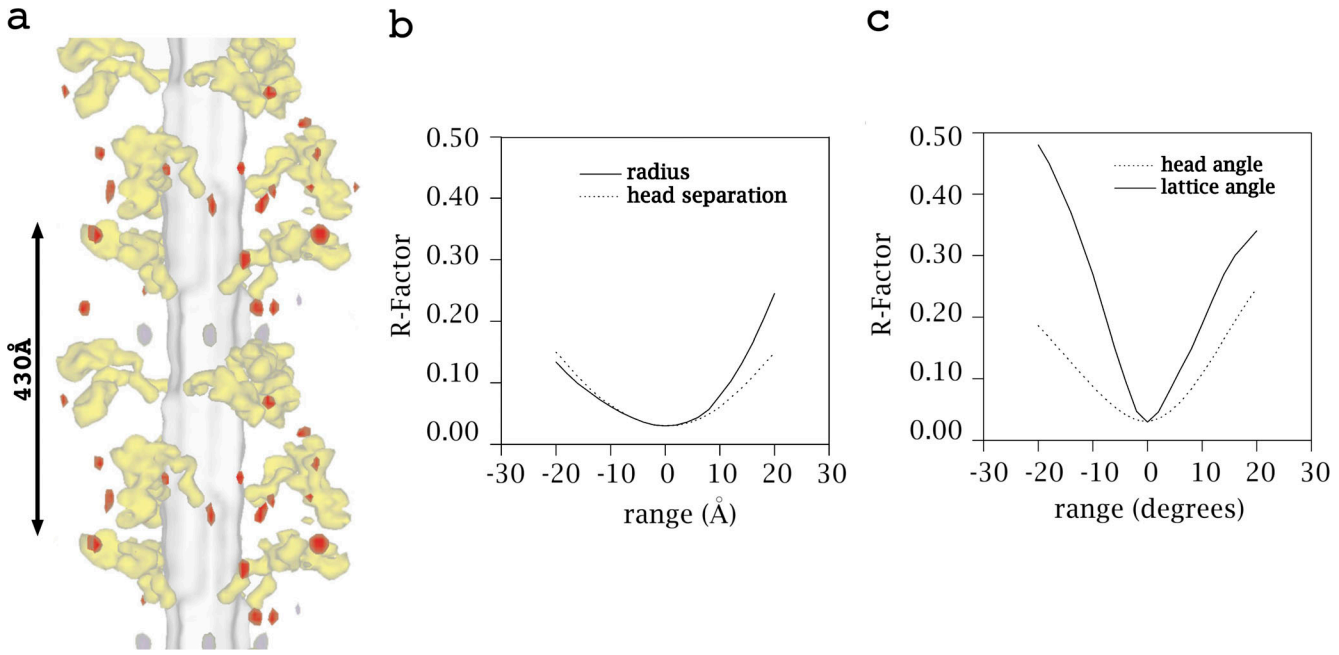

Figure 4. **Fourier difference synthesis and R-factor plots. (a)** The best model of the bony fish muscle myosin filament in the relaxed state (data from the work of Hudson et al., 1997). Myosin heads are yellow on a gray backbone. The red and gray patches are from a Fourier difference synthesis (see text) showing where the difference density is positive (red) or negative (gray). The amplitudes of the difference densities are in fact very low, indicating that the model itself is a good one. **(b and c)** The sensitivity of the R-factor used in the modeling in a to variations in certain parameters. The central points (0) in the plots represent the R-factor values for the best model as in a, and the variations show the changes in the R-factor as one particular parameter is changed while all others are kept fixed at their optimal values. Very small parameter changes can cause large increases in the R-factor, showing that these parameters are important ones. If there had been no change, then the observations would not justify inclusion of that particular parameter in any modeling.

rotational symmetry (Squire, 1972) and no radial perturbation, this gives one value of R and 3 parameters for each of the 6 nonequivalent heads in a 430 Å repeat, a total of 19 parameters. If the head shape is allowed to alter as well, such that the lever arm is one object and the motor domain is another that can rotate on the lever arm, then there are 3 more parameters (azimuthal tilt, axial tilt, and rotation of the motor domain around its axis) per nonequivalent head, or 18 more parameters, for a total of 37 parameters. An additional parameter is the rotation of the whole filament around its long axis relative to the unit cell sides, 38 parameters in all, ignoring any disorder parameters. These parameters were refined by Hudson et al. (1997) and later by AL-Khayat and Squire (2006) by modeling against 56 observed independent intensities. The quality of the model was tested using an objective goodness-of-fit factor or R-factor, which compared the observed and calculated intensities. It was found that at the resolution being considered, out to ~72 Å, inclusion of slight axial, radial, or azimuthal origin perturbations had little effect on the goodness of fit, so not including them was justified. The weighted R-factor used by Hudson et al. (1997), which is a satisfactory one to use in muscle modeling, was:

$$R = \frac{\sum_{i=1}^{N} (I_i^o - I_i^c)^2 / \sigma_i^2}{\sum_{i=1}^{N} (I_i^o)^2 / \sigma_i^2},$$

where I^o is the observed intensity, I^c is the calculated intensity, N is the number of observations, i denotes a particular observation, and σ_i denotes the SD associated with the measurement of I_i^o. The inclusion of σ_i means that observed intensities that are less reliable than others are down-weighted in the R-factor calculation. If σ_i values are not available, then both of the σ_i^2 factors can be removed from the R-factor expression above, and reflections will be considered as equally accurate (i.e., put $\sigma_i^2 = 1$).

The preferred myosin filament structure by Hudson et al. (1997) is shown in Fig. 4 a. One of the advantages of using data from highly sampled (almost crystalline) diffraction patterns is that there are tricks one can play to test the structure. For example, the model and observed intensities, even with the best model, will be slightly different. However, since we have a model, the phases of the diffraction peaks can be calculated, the relative intensities of overlapping peaks can be estimated, and the amplitude (square root of intensity) differences can be used with the calculated phases to generate a new "difference" density map by Fourier synthesis. Such a map for bony fish muscle is also shown in Fig. 4 a. The density differences, both positive and negative (see red and gray patches), show where density should be moved to or from, but the actual difference density values were found to be rather small, providing confidence in the "best" structure, as shown in the main part of Fig. 4 a.

In recent times, nearly all isolated myosin filaments seen in electron micrographs and analyzed by single-particle analysis have shown the presence of the interacting head motif (IHM; Wendt et al., 1999; Hu et al., 2016; Lee et al., 2018; Daneshparvar et al., 2020). Analyses of x-ray patterns from vertebrate skeletal

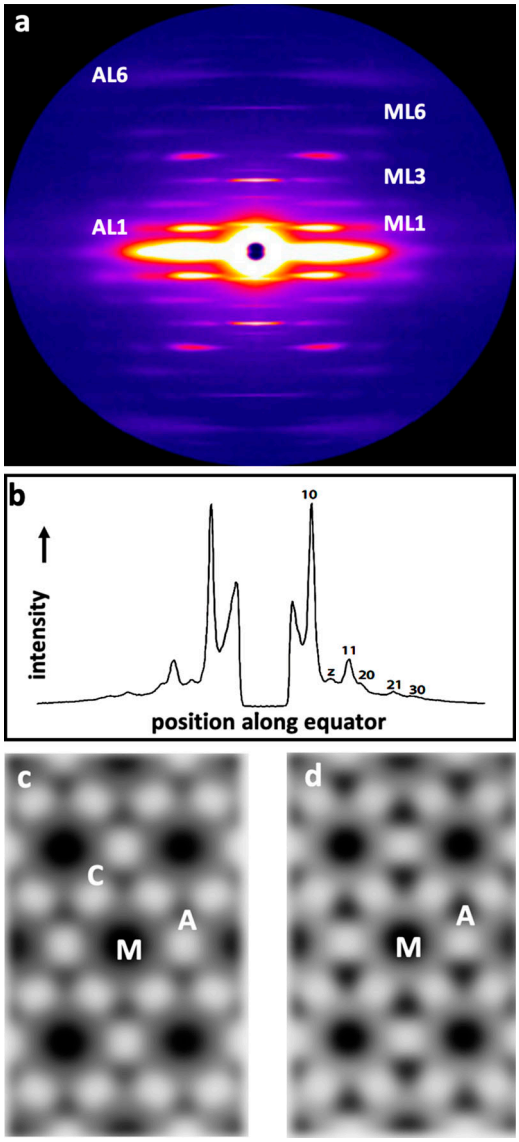

Figure 5. **2-D diffraction patterns and Fourier syntheses. (a)** The beautiful low-angle x-ray diffraction pattern from tarantula muscle from Padrón et al. (2020) showing myosin filament layer lines ML1, ML3, and ML6 and actin layer lines AL1 and AL6. Like vertebrate muscle, ML3 is at ∼145 Å, but the myosin filaments are four-stranded, not three-stranded as in Fig. 4 a. The layer lines are completely unsampled. Reprinted with permission from Padrón et al. (2020). **(b)** The symmetrical intensity profile along the equator of the low-angle x-ray diffraction pattern from bony fish muscle. The 10, 11, 20, 21, and 30 peaks come from the hexagonal unit cell of the myosin and actin filaments in the A-band, and the peak marked Z comes from the almost square lattice of actin filaments and α-actinin in the Z-band. **(c and d)** Electron density maps of bony fish muscle viewed down the fiber axis and calculated from the equatorial peaks out to the 30 peak: c from relaxed muscle and d from fully active muscle. Cross-bridge density (C) moves from around the myosin filaments (M) in resting muscle (c) toward the actin filaments (A) in active muscle (d). Data from Harford et al. (1994).

and insect flight muscle by Knupp et al. (2019) and AL-Khayat and Squire (2006) led to the suggestion that the IHM structure is present in some physiological conditions, possibly forming the superrelaxed (SRX), low–ATP use state (McNamara et al., 2015; Tolkatchev et al., 2018), but in normal resting bony fish muscle, a different structure appears to predominate. The IHM structure has the heads compactly against the filament backbone (a "heads in" structure), whereas in the model by Hudson et al. (1997), it has the heads projecting further outward (a "heads out" structure). If this is real, then it is not known what causes the transition in the muscle, from the SRX (heads in) to the normal relaxed (heads out) state, although treatment with mavacamten can increase the IHM content (Nelson et al., 2020).

The elegant study by Nelson et al. (2020) has suggested that there may be a mixed population of head states in relaxed vertebrate skeletal muscle, with the SRX state, presumably the IHM structure, being ∼28% of the total. Further modeling of relaxed muscle with a mixed head population, mostly heads out, but with a small proportion of IHM heads, is warranted and may help to determine even more accurately the head conformation in the heads out structure.

Finally, in doing modeling, it is necessary to test the appropriateness of the parameters that have been chosen. It may be that there are some parameters in a particular analysis that have very little effect on the region of the diffraction pattern that is being modeled. This is very easily tested. Fig. 4, b and c, shows the sensitivity of the R-factor in the analysis of Hudson et al. (1997) to various parameters. The center of each plot shows the R-factor for the best model (Fig. 4 a), and the rest of each plot shows how the R-factor changes when one particular parameter is altered with all other parameters kept fixed at their optimal values. Clearly, the R-factor is very sensitive to the values of these particular parameters. If the same kind of thing had been done and the result were that the R-factor did not change, then the parameter being checked would essentially be redundant, its value could be fixed, and it should not be included in any further parameter search. In this way, the choice of appropriate adjustable parameters can be optimized.

Test case 3: Modeling myosin filaments in relaxed noncrystalline muscles

Modeling myosin filament structure from x-ray diffraction patterns from muscles that do not have the beautiful crystalline order of fish muscle or insect flight muscle is much more difficult. An example is the layer-line pattern from tarantula leg muscle (Fig. 5 a; Padrón et al., 2020). In its way, it is also a beautiful pattern, but in this case, the layer lines are not sampled. In a sampled diffraction pattern, one knows that the observed peaks arise from the structure when viewed down particular lattice planes through the unit cell. In the case of unsampled fiber diffraction patterns such as that in Fig. 5 a, the layer lines are cylindrical averages of everything on that layer line, and it is not possible to determine how much the structure under test diffracts in particular directions.

What has to be done here is to compare the general profile of the layer lines with the cylindrically averaged profiles computed from model structures. Of help is the fact that the myosin head arrays in these muscles appear to be perfectly helical; there is no perturbation. The problem is that there are probably many structures that will give the same cylindrically averaged diffraction patterns. Padrón et al. (2020) claimed that the observed layer-line intensity distribution is well explained by the IHM

structure for tarantula, based on their EM reconstruction (Woodhead et al., 2005). This may be true, although the fit is not perfect, but, at best, they could claim that the pattern is consistent with the observed layer-line pattern. It would not be justified to claim that the IHM structure has been proved by x-ray analysis to be the structure present in relaxed, intact tarantula muscle. A more detailed analysis with a model where the head positions can be adjusted would be needed to do this, and this would show how sensitive the fit is to cross-bridge position. In other words, in doing, for example, a simulated annealing search for the best parameters, it may well be that there are several sets of parameters (i.e., different structures) that give virtually the same R-factors. This is a real problem that emphasizes the advantages of studying highly ordered tissues such as bony fish and insect flight muscles.

Test case 4: Determining cross-bridge movements in active muscle using the equator as a tool and by modeling

The equator of the diffraction pattern, the horizontal line of spots through the centers of the patterns in Fig. 1, provides information about sarcomere structure when viewed down the fiber axis. A typical equatorial intensity profile from vertebrate striated muscle is shown in Fig. 5 b. Most of the peaks come from the A-band lattice, but some do come from the Z-band as well. Classically, the A-band equatorial intensities have been used to monitor cross-bridge position in different muscle states because the inner two peaks, the 10 and 11 reflections, change their relative intensities in a reciprocal way in patterns from resting muscle, active muscle, and rigor muscle (Haselgrove and Huxley, 1973; Yu and Brenner, 1989; Harford and Squire, 1992; Harford et al., 1994). The 10 peak gradually reduces and the 11 peak gradually increases through these three states. Rigor vertebrate muscle has ∼100% of the myosin heads attached to actin (Cooke and Franks, 1980; Lovell et al., 1981), so to a first approximation, the number of attached heads in other states is often assessed relative to rigor in terms of the intensity ratio I_{11}/I_{10}. However, it should be remembered that this is a relatively crude way of assessing attachment number, because it is known that two muscles with the same proportion of actin-attached heads, but with the heads in different configurations on actin, can give quite different I_{11}/I_{10} ratios (Lymn, 1978). We confirm this later and also discuss an alternative to using the I_{11}/I_{10} ratio.

If there are enough equatorial reflections to use, often up to five for vertebrate muscle, namely the 10, 11, 20, 21, and 30 reflections, then it is possible to calculate electron density maps by Fourier synthesis from the measured intensities and using estimated phases. Because, at the resolution being considered (the 30 spacing is ∼130–140 Å), the structure being studied is almost centrosymmetric (density the same at +x,+y and −x,−y in projection down the fiber axis onto the equatorial plane), the phase angles cannot have any value between 0° and 360° but are restricted to being 0° or 180°. These correspond to phase factors in different terms of the Fourier synthesis expression of +1 or −1. It has been found that phase sets +1, +1, −1, +1, +1, or +1, +1, −1, −1, +1 give the most sensible distributions of density in the vertebrate muscle unit cell compared with other combinations (Fig. 5, c and d; Yu and Brenner, 1989; Harford and Squire, 1992; Harford et al., 1994).

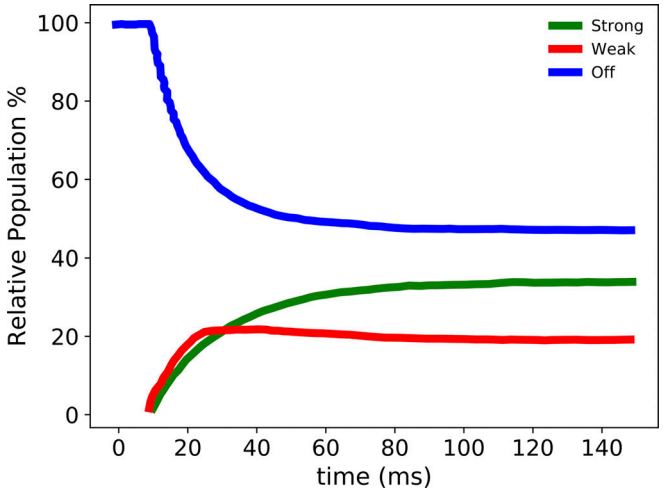

Figure 6. **The changing populations of the three myosin head states modeled by Eakins et al.** The tension time course follows a similar trend to the strong. Adapted from Eakins et al. (2016).

Moving now to studies of the equator in time-resolved x-ray diffraction studies through, for example, a tetanic contraction (Haselgrove and Huxley, 1973; Huxley and Kress, 1985; Harford and Squire, 1997; Hoskins et al., 2001; Eakins et al., 2016) or after ATP release (Tsaturyan et al., 1999), it is possible to monitor cross-bridge movement and cross-bridge configuration in a systematic way. For example, Eakins et al. (2016) studied the time courses of equatorial reflections out to the 32 peak (∼90 Å resolution) during tetanic contractions of bony fish muscle and were able to model the observed changes in terms of a simple cross-bridge structural cycle. This cycle is often thought of as including a weak binding state (Brenner et al., 1982; Yu and Brenner, 1989) similar to a prepowerstroke state (Houdusse and Sweeney, 2016), followed by one or more strongly binding, force-producing states, after which the bridges bind ATP, detach from actin, then hydrolyze the ATP to ADP and P_i, making them ready for a further cycle of weak binding and so forth (Lymn and Taylor, 1971). Eakins et al. (2016) found that they could model the observed equatorial intensity changes well using a three-state cycle with two attached states, one an initially attached state not unlike the weak binding state in its effect on the equator and one strong, force-producing state such as the rigor state in its effect on the equator. The populations of states are shown in Fig. 6. Happily, to do this, they only needed the amplitudes (square root of intensity) and not the phases of the equatorial peaks. The number of parameters they were trying to fit was significantly less than the number of observations. They also tested models with more states and found that the inclusion of extra states did not significantly improve the fitting of the observations. This is another way of testing the reliability of any conclusions. If you add further complexity to a model without improving the fit, then inclusion of the further complexity is not justified by the data.

One of the conclusions from the time-resolved equatorial analysis by Eakins et al. (2016) was that the changes in the 11 intensity, which were ahead of the 10 change and tension (Fig. 7

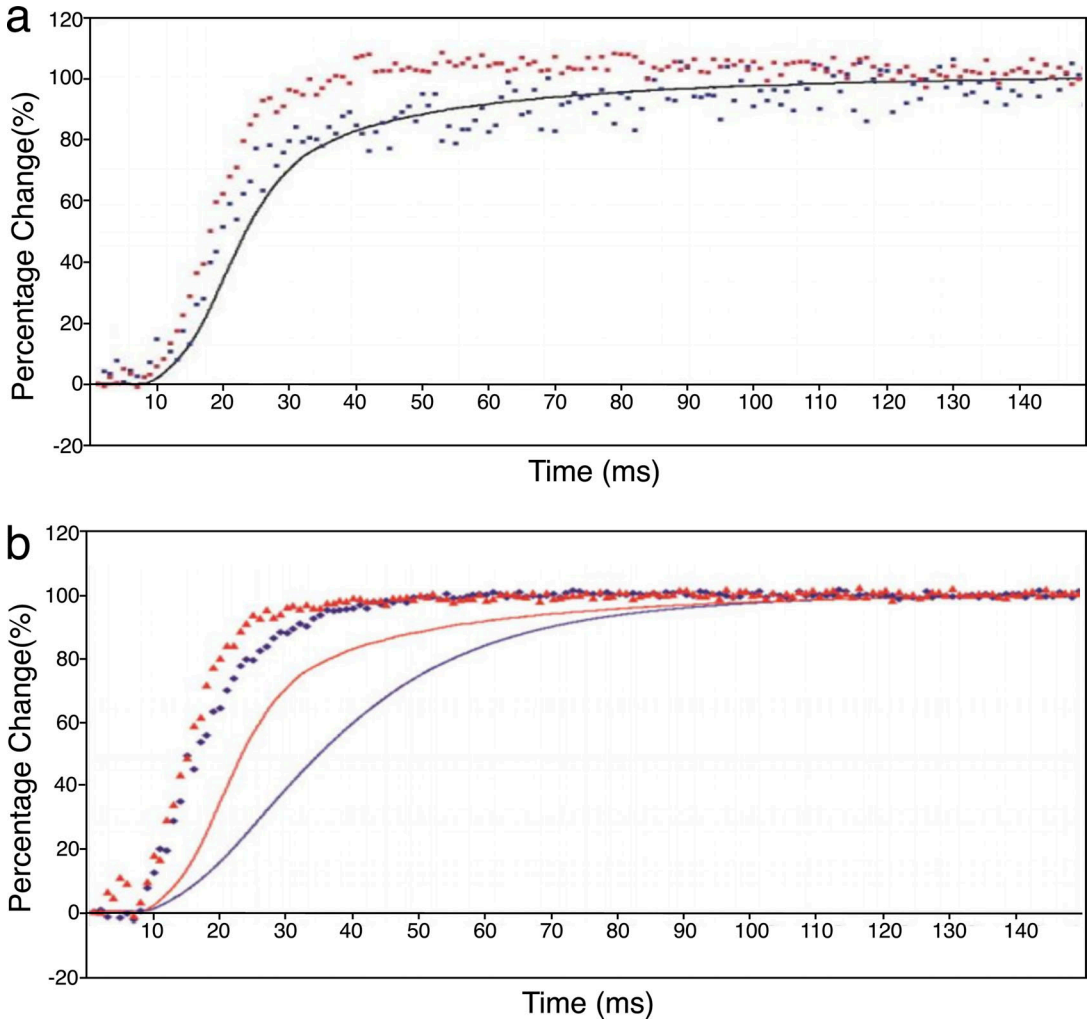

Figure 7. **Time courses of the 10 and 11 equatorial reflections from bony fish muscle. (a)** The different time courses of the equatorial 10 (blue dots) and 11 (red dots) peaks from contracting bony fish muscle relative to tension (solid line) from Eakins et al. (2016). **(b)** The time course of the intensity ratio I_{11}/I_{10} (dots) compared with tension (solid lines) from bony fish muscle without sarcomere length control (black) and with partial sarcomere length control (red). In neither case does the intensity ratio coincide with the tension trace. Reproduced from Eakins et al. (2016).

a), were largely due to the weak binding or initially attached state, and that the occupancy of the rigor-like or strong state had a similar time course to the tension and the 10 peak. In other words, there is a cross-bridge state (or mixture of states) on actin similar to the weak binding state in its effect on the equator, which is occupied ahead of tension production, followed by an attached state (or a mixture of states), not significantly different from the rigor state in its effect on the equator, associated with tension production. In addition, the fact that the 10 and 11 peaks have different time courses emphasizes that they are not just dependent on the number of attached heads; as mentioned earlier, the head configuration on actin also has a significant effect on the I_{11}/I_{10} ratio (Lymn, 1978). Fig. 7 b shows the variation of the I_{11}/I_{10} ratio with time (symbols) compared with that of tension (solid lines) for fish muscles with and without partial sarcomere length control. The time courses are clearly very different. The relative intensity changes of the 10 peak on its own (Fig. 7 a) appear to be a better measure of the number of attached force-producing heads than the I_{11}/I_{10} ratio, although in a reciprocal way; the 10 intensity drops as more heads are attached. This is supported by the experiments of Reconditi et al. (2014), who show in their Fig. 3 A a linear relationship between 10 intensity and tension. Similarly, the 11 time course is a better indicator of the initially attached population.

Finally, note that the diffracting characteristics of the weak and strong are such that it is very clear that the myosin heads have different configurations on actin in the two states (Eakins et al., 2016). The way the motor domains label actin may be different or the axial tilt of the lever arms may be different in the two cases. For example, a change in lever arm axial tilt between the weakly and strongly attached states could take the head mass closer to the actin filament and explain why the equatorial pattern changes.

Test case 5: The meridional diffraction pattern

The meridian of the diffraction pattern has superimposed contributions from every single component of the sarcomere. In patterns from resting muscle, there are peaks from the cross-bridge

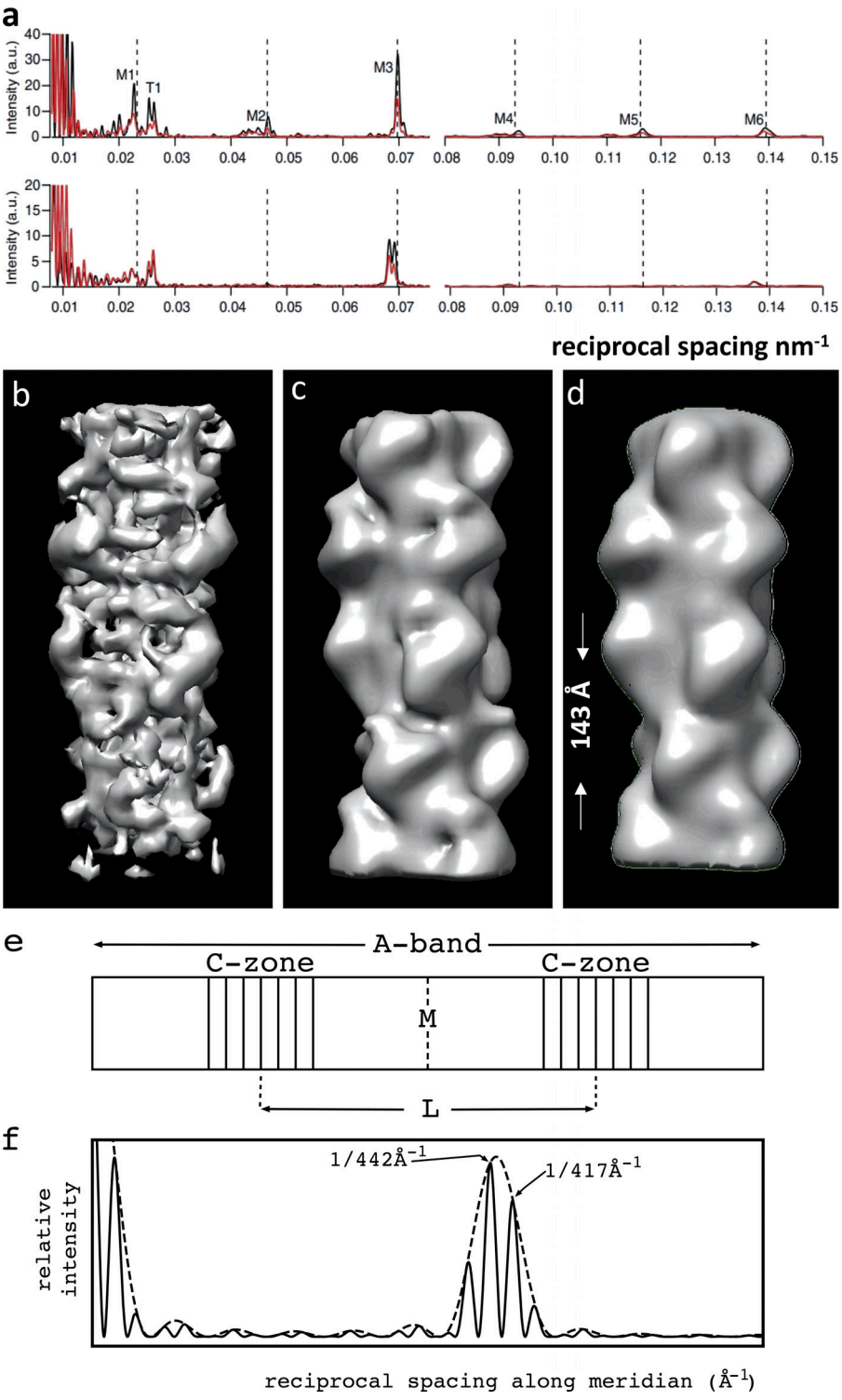

Figure 8. **Meridional reflections and interference effects. (a)** Intensity profile along the meridian from frog muscle in the relaxed (top) and active states (bottom). a.u., arbitrary units. Reproduced from the work of Reconditi et al. (2014). Reflections from myosin are labeled M1, M2, and so forth. T1 comes from the troponin–tropomyosin complex. The fine sampling of the diffraction patterns comes from interference between the diffracted x rays from the two halves of the A-band as in e and f for C-protein. Peaks to the left of each trace are from the sarcomeres acting as diffraction gratings and give a direct measure of sarcomere length at least up to sarcomere length ∼3.0 µm. **(b–d)** 3-D reconstruction of the human cardiac muscle myosin filament shown at three different resolutions. b is the original map of AL-Khayat et al. (2013), c is the same structure shown at 72.5 Å resolution for active muscle, and d is shown at 145 Å resolution. c and d show the very low level of detail that might be expected from analysis of the M6 (∼72.5 Å) and M3 (∼145 Å) reflections alone. Figures courtesy of Dr. Edward Morris. **(e and f)** Analysis of the meridional peaks from C-protein around M1 along the meridian of diffraction patterns from some muscle types. The middles of the two C-zones in e are separated by the interference distance L. C-protein is a myosin filament protein and occurs on every third crown at a spacing of ∼430 Å in resting muscle. However, the outer part of C-protein can extend across to actin (Squire et al., 2003; Luther et al., 2011), where it binds, on average, at a slightly different spacing of ∼440 Å. The net effect is a C-protein meridional peak from one-half A-band at ∼434 Å. For some muscles, this is then sampled by the interference function to give two unequal peaks, one at ∼442 Å stronger than one ∼417 Å (f). In other muscles, with a slightly different interference spacing L, an interference peak is almost coincident with the center of the underlying C-protein peak, and a single strong M1 peak is seen (e.g., as in a). Reproduced from Squire et al. (2003).

array on the myosin filaments, which, as discussed above, could have a mixture of heads in and heads out conformations, peaks from the distribution of C-protein (myosin-binding protein-C), and peaks from the myosin filament backbone, including titin. In the case of vertebrate striated muscles, there are contributions from the actin helix on one axial repeat and the tropomyosin/troponin system on a different repeat. In patterns from active muscle, all of these things still diffract, but possibly in different ways from before, and, in addition, some of the heads originally on the myosin filament backbone will now be binding to actin monomers in a variety of conformations and with an unknown axial distribution of the actin monomers that are labeled. The second heads of molecules attached to actin will probably have changed their conformation, too. These changes will require modeling that uses more parameters than for resting muscle. To complicate matters still further, the diffraction

from the bridge regions in the two halves of the A-band will interfere, giving rise to interference functions of different periodicities depending on, for example, whether the myosin heads are myosin-centered or actin-centered or on the separation of the C-proteins across the A-band. The reflections from tropomyosin/troponin will also be sampled by an interference function, but this time it is likely to be due to interference between the two halves of the actin arrays across the Z-band (Squire, 1981, pp. 362–363). If it is remembered also that different sarcomeres in a muscle will have slightly different sarcomere lengths, giving slightly different head-labeling patterns on actin in different sarcomeres, and that diffraction from all sarcomeres will superimpose to give what is recorded in the diffraction pattern, then some idea of the complexity of the meridian will become clear.

Fig. 8 a, from Reconditi et al. (2014), shows intensity traces along the meridian from frog muscle that is relaxed (top) or fully active (bottom). Here the meridional peaks with contributions from the myosin filaments (e.g., cross-bridges, backbone, C-protein, titin) are labeled M1, M2, and so forth. These are mostly orders of the myosin filament repeat of ∼430 Å in the relaxed pattern, with the M3 peak at ∼143 Å, associated with the crown separation along the myosin filaments (Fig. 8, b–d), being particularly strong. The peak labeled M1 is mainly due to C-protein, on a slightly longer axial repeat (∼434 Å), as is some of the M2 peak (see discussion below in this section). In addition to these myosin-based periodicities, the peaks labeled T1 are from the tropomyosin/troponin complex of axial repeat ∼385 Å. Higher orders of this repeat are sometimes seen as well. All of these meridional peaks are multiplets in the sense that they have been sampled by their own interference functions (see below).

Comparing the patterns from relaxed and active muscle (Fig. 8 a) shows significant differences. The M1 peak is weak in the pattern from active muscle (top panel), perhaps suggesting some disordering of the C-protein. In relaxed muscle, C-protein is thought to be anchored to the myosin filament backbone by its C-terminal domains (C7–C10), but to stretch across to bind to actin through its N-terminal domains. Release of C-protein from actin in active muscle could allow it to become disordered and thus reduce the M1 peak (Squire et al., 2003).

Looking at the M3 and M6 peaks in Fig. 8 a, both have smaller peak heights in the active pattern (lower panel), and both shift toward the left (toward longer spacings). At the same time, the M3, which started as a single peak with satellites, is a clear doublet of nearly equal peaks in the active pattern. Some of these axial shifts appear to be due to activation of the myosin filament in some way, which shifts the crown repeat of ∼143 Å to a spacing that is 1.0–1.5% longer (Haselgrove, 1975; Reconditi et al., 2014). In addition, when force is generated, the actin and myosin filaments both stretch elastically by ∼0.2–0.3% at maximum tetanic force (Huxley et al., 1994; Wakabayashi et al., 1994; see Knupp and Squire, 2019; see also Ma et al., 2018 for recent experiments showing that thick filament can extend up to 1.2%). Not obvious is that the width across the meridian of the M3 goes up as well, so the total intensity in the M3 peaks is actually higher in patterns from active muscle than resting muscle (for discussion, see Eakins et al., 2019). There is evidence in patterns from active muscle that the M3 has at least two components with different widths across the meridian, a sharp peak (M3m) which is similar in width to the resting M3 peak, and a broader peak (M3a), probably due to actin-attached cross-bridges (Eakins et al., 2019). The M3a peak broadening is probably due to the actin filaments to which the cross-bridges are attached being more laterally disordered than the myosin filaments in active muscle.

Considering these various meridional contributions in more detail, we use the C-protein array as an example of the effects of interference. Fig. 8 f shows diagrammatically how a broad diffraction peak at ∼434 Å is sampled by closely spaced fringes due to interference between the diffraction patterns from the two C-zones in one A-band (Fig. 8 e) separated by the interference distance L. Fig. 8 f shows interference fringes at ∼442 Å and ∼417 Å, with the 442 Å peak being the stronger of the two. The relative strengths of the two peaks depend on the length of the C-zone and the exact value of L. Some C-zones have seven C-protein stripes, and others have more, up to nine, and the M1 pattern will vary accordingly (Sjöström and Squire, 1977; Bennett et al., 1986). Fig. 8 a (top) has a relatively strong M1 peak with a satellite on its left (longer spacing), probably due to a longer C-protein array in frog muscle than in the human tibialis anterior muscle reproduced in Fig. 8, e and f (Squire et al., 2003).

Considering the effects of C-protein on the meridian in more detail, very careful analysis was performed by Squire et al. (2003) on the effects of actin binding by C-protein. One of the curious observations in the past was that, although C-protein was known to be a myosin-binding protein, as we have seen, the main meridional reflection known to come from C-protein (Rome et al., 1973a; M1 in Fig. 8 a) always showed a slightly longer spacing than the myosin filament axial spacing of close to 430 Å in relaxed muscle. Squire et al. (2003) showed that only if C-protein was also binding to actin, and only if there was a limited number of stripes of C-protein, as delimited by the C-zone, would the meridional peak from C-protein be at a longer spacing than the myosin repeat. They found that, as in Fig. 8 f, the C-protein stripes in one half A-band would give a meridional peak at ∼434 Å only if the C-protein extended across to actin and labeled actin in a specific way. There is now direct evidence for actin labeling by C-protein (Luther et al., 2011). C-protein molecules binding to myosin with the myosin repeat of 430 Å would extend across to actin and bind there with an ∼440 Å spacing to give the observed 434 Å average spacing (440 Å is eight times the 55 Å actin monomer repeat along the long period strands; see Fig. 3 a). As discussed above, diffraction from the C-zones on opposite sides of the same A-band would then interfere to give sharp C-protein peaks. It is a quirk of the A-band structure that if the C-zone had been much longer in the axial direction, then the C-protein peak would have averaged out to 430 Å, not 434 Å.

Note, finally, that if the C-protein stripes of density have a roughly Gaussian density profile in resting muscle in projection onto the fiber axis, then it may well be that C-protein contributes not only to the M1 peak but also to M2 and possibly M3 as well (Fig. 9 a).

Test case 6: Modeling cross-bridge behavior in resting and active muscle from the meridian

We have seen from Fig. 4 a and the earlier discussion of modeling the myosin layer lines that the dominant heads out

configuration in relaxed muscle can be modeled satisfactorily (Hudson et al., 1997). In the future, this can be refined to include the small heads in population, but the techniques to do this are defined. This modeling depended on not only the relative conformations of the two heads of one myosin molecule but also the differences between the three different crowns of heads within a 430 Å repeat. This difference is the well-known axial perturbation in the vertebrate muscle myosin filament (Huxley and Brown, 1967; Harford and Squire, 1986; Fig. 4).

Fig. 9, a–c, illustrates the sort of effects on the meridian that the axial perturbation can have (Squire et al., 1982). The bottom panels show a set of Gaussian density profiles on a 429 Å axial repeat but with different intercrown axial separations *a*, *b*, and *c*. Fig. 9 b has $a = 153$ Å, $b = 113$ Å, and $c = 163$ Å, whereas Fig. 9 c has $a = 163$ Å, $b = 128$ Å, and $c = 138$ Å. This difference has a profound effect on the meridian. Even though the cross-bridge shapes and total density in the two cases are exactly the same, (b) has a weaker M3 peak and gives M5 > M4, whereas (c) has a much weaker M2, a stronger M3 and M5 < M4. If there was no perturbation, then M2, M4, M5, and all further orders not multiples of 3 would have zero intensity. This is an example of having the same head conformation and head density but changing the diffraction pattern radically by altering the axial distribution of the heads.

Going on to diffraction patterns from active muscle, what will be the important factors there? First of all, some of the heads that were originally organized on the myosin filament and that are myosin centered (i.e., the heads in and heads out populations) will move out and attach to actin, where they may be weak binding heads, or prepowerstroke heads, or heads at the end of their working stroke, and some in between. In addition, they may be the second heads of heads attached to actin. There will be heads on actin with different conformations and heads left on myosin in conformations that may be different from the relaxed heads in and heads out structures. Apart from this, we do not know the axial pattern of labeling of heads on actin, and within that pattern, we do not know which myosin head structures will be on which actin monomers.

As in Fig. 9, b and c, for relaxed muscle, the axial distribution of heads on actin in active muscle will also have a profound effect on the intensity of the M3 and other meridional peaks. In addition, the elastic lengthening of the myosin and actin filaments under tension will alter the interference functions, with the myosin and actin lengths changing by differing amounts. The take-home message here is that, like it or not, the muscle meridian is extremely complicated, and unscrambling all the different factors is no easy task.

Knupp et al. (2009) carefully analyzed the M3 interference data of Dobbie et al. (1998), Bagni et al. (2001), Linari et al. (2000, 2005), Irving et al. (2000), Piazzesi et al. (2002, 2007), Lombardi et al. (2004), Reconditi et al. (2003, 2004, 2005), Ferenczi et al. (2005), Brunello et al. (2006), Colombini et al. (2007), and Huxley et al. (2006a, 2006b). These many authors claimed that by analysis of the changing M3 and M6 intensities and the change in the interference fine structure of these peaks, they could monitor the behavior of the lever arms of the myosin heads. Knupp et al. (2009) did not agree with this. The conclusion

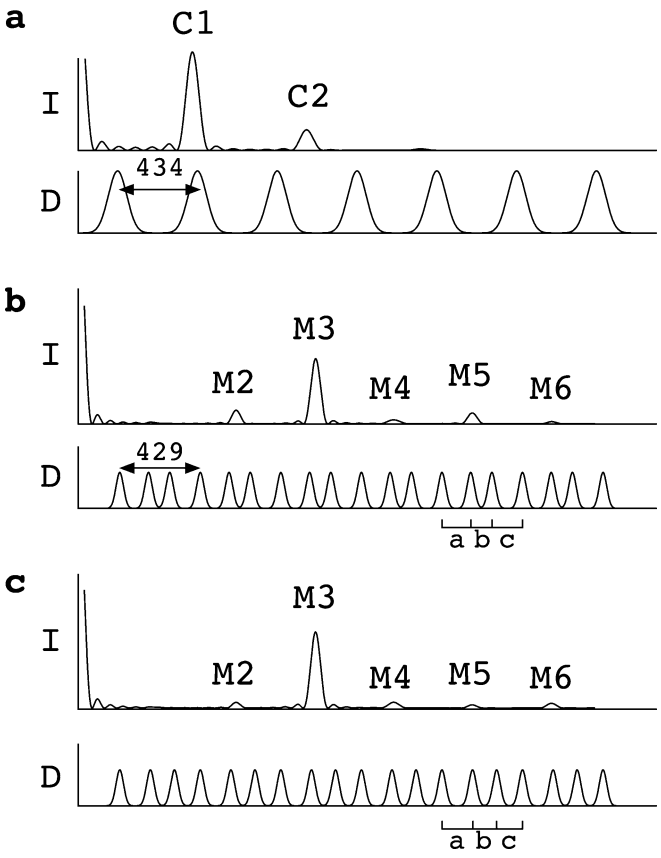

Figure 9. **Effects of axial perturbations on the meridional reflections. (a–c)** Lower plots: Possible densities along myosin filaments in vertebrate striated muscles. **(a)** C-protein represented as Gaussian peaks every 434 Å (D, protein density; I, x-ray intensity). **(b and c)** Two different sets of myosin crown spacings *a*, *b*, and *c*, with systematic perturbations of the basic 143 Å crown repeat. Upper plots: Calculated diffraction intensities along the meridian for the different density profiles in the lower plots. Note that in a, there is a main C1 peak at 434 Å, but there may be C-protein contributions (C2) close to the M2 and beyond, depending on the C-protein density profile. Note in b and c that the relative intensities of the M2–M6 peaks depend very much on the particular axial perturbation that is involved. In both cases, the crown density profiles and weights are exactly the same. All the observed differences in the diffracted intensities are due to the relative axial shifts of the crowns. For discussion, see text. Reproduced from Squire et al. (1982).

of Knupp et al. (2009) was much as we have stated above; if the number of observations is less than the number of parameters needed to model the observations properly, then no reliable model can be deduced; the problem is underdetermined. In addition, if the resolution is too low and the number of peaks being analyzed is small, then great care needs to be taken about what is claimed. Using a variety of specific examples, Knupp et al. (2009) showed that the same data as published by the authors listed above could be modeled equally well in several different ways, including models that did not involve any rotation of the lever arms.

The reason that the observations are insufficient to define lever arm movement is simple. First, the M3 reflection has a spacing of ~143–146 Å; it is providing very low-resolution information. Second, there is no information whatever about the shape of the diffracting object in a single peak such as the M3,

except to say that there is an indeterminate blob of mass at this axial spacing. Third, if the M6 is included and there is general agreement that only some of the M6 comes from the myosin heads, the rest being from the backbone, there is slightly more information about the shape of the diffracting object, but not much. Knupp et al. (2009) showed that Gaussian density profiles representing the motor domains of myosin heads on actin and other Gaussian shapes representing heads ordered back on the myosin filament backbone could explain all the M3 and M6 observations from the experimental papers listed above, without any thought about what the lever arm might be doing. This was confirmed directly by using all the M3 and M6 meridional information, including the intensities of the inner and outer interference peaks, to generate electron density maps by Fourier synthesis. These showed the relative movement of two roughly Gaussian shapes spaced at 145 Å and moving relative to each other as the actin filaments moved past the myosin filaments. The crucial point here is that there is no other information in these M3 and M6 peaks than is carried in the Fourier synthesis. The take-home message is that the M3 and M6 peaks, including the interference peaks, on their own carry much less information than is necessary to monitor the behavior of the lever arms or to define other details of the myosin heads.

This conclusion is reinforced by images such as those in Fig. 8, b–d. Here, the electron density map of the human cardiac muscle myosin filament obtained by AL-Khayat et al. (2013) is shown at three different resolutions. Fig. 8 b shows the published density map at the highest resolution that could be achieved. Courtesy of Dr. Edward Morris (Institute of Cancer Research, London, UK), this same map is then shown in Fig. 8, c and d, at gradually reducing resolution. Fig. 8 c is filtered to 72.5 Å resolution and Fig. 8 d to 145 Å resolution. These show the sort of level of detail that one is dealing with in studying the M3 and M6 reflections.

We show below that to explain the behavior of the M3 and M6 meridional peaks in a sensible way, it is necessary to generate quite a sophisticated model at higher resolution, including all the factors that have been discussed above, and to solve this model, it is necessary to analyze very much more of the diffraction pattern than just the M3, M6, and ML1 peaks. It is not apparent to us that there is any way to use the M3 and M6 peaks on their own as tools to monitor specific head configurations in the cross-bridge cycle.

Discussion: Some suggested basic rules

In summary, the low-angle diffraction region of the fiber diffraction patterns from different muscles provide a wealth of important information about muscle structure and how muscle works. However, interpretation and modeling of the observed patterns needs to be performed with great care, and claims about the interpretation of the data should not go beyond what can really be objectively justified.

We recognize two different ways of using x-ray diffraction observations. One is to use x-ray diffraction as a tool to monitor particular features of the muscle unit cell, and the other is to use modeling to try to understand structural mechanisms in the cross-bridge cycle.

X-ray diffraction as a tool

The x-ray diffraction technique is superb at determining changing filament axial spacings or lattice spacings. It can also provide a very good measure of the sarcomere length. Fig. 8 a from Reconditi et al. (2014) has peaks very close to the center of the pattern, fully to the left of these profiles, which come directly from the muscle sarcomeres behaving as diffraction gratings. These peaks show directly what the sarcomere length is. This is a wonderful technical advance on what could be done before and really helps to define what is going on. The sarcomere length signal comes from exactly the same part of the muscle and the rest of the diffraction pattern. In addition, as we have seen, the 10 and 11 equatorial peaks can be used to estimate the number of actin-attached heads, with the reciprocal of the 10 intensity probably a better indicator than the 11/10 ratio of the presence of force-producing heads. The 11 intensity seems to be a good indicator of the initially attached (weak or prepowerstroke) myosin head population.

Parts of the meridian can also be used as a tool. The spacings of some of the higher-order meridional peaks, such as the M15 peak from myosin and the A13 from actin, because they are so far out from the center of the diffraction pattern, can be measured very accurately (also note that the M6 spacing is not as problematic to interpret as its intensity). Huxley et al. (1994) and Wakabayashi et al. (1994) used these peaks and others to show the elastic change of length of the myosin and actin filaments due to tension generation in active muscle (see analysis in Knupp and Squire [2019]; see also the papers by Ma et al. [2018] and Kiss et al. [2018], expanding on the work by Huxley et al. [1994] and Wakabayashi et al. [1994]). However, as we have detailed above, the M3 and M6 peak intensities and even the ML1 layer line cannot be used as a simple tool. Wherever possible, information from the whole diffraction pattern should be analyzed.

Ways to model the cross-bridge cycle

If particular diffraction information cannot be used as a tool to monitor specific structural changes, then modeling is needed. Ideally, muscle diffractionists should have an idea in their minds before designing and starting their experiments about what outcome they wish to achieve. They will usually know the diffraction properties of their muscle pretty well, so they can assess how much of the diffraction pattern they will need to record to provide enough observations that they can do the required reliable modeling using fewer adjustable model parameters than observations.

Going on to how to model structural changes in a muscle, the authors have shown that the equatorial pattern (Fig. 5 b) can be modeled to show how many main structural states there are and what their changing populations are through a tetanic contraction (Fig. 6). In doing this, they have used more observations than parameters.

But if we wish to define fully what the cross-bridges are doing in active muscle in 3-D, we need to be rigorous and to use as much of the whole diffraction pattern as possible. As a guide to producing modeling results that can be justified, here are some suggestions. (1) Record x-ray diffraction data from muscle

Table 1. **M3, M6, and ML1 observations and parameters**

Observations					**Parameters needed to model M3 and M6 fully**	
Relaxed muscle						
M3	IM3i			1	Lattice of head array on myosin	Known
	IM3o			1	Configuration of heads on myosin assuming random occupancy	(7–13[a]) × 2
	dM3i	~143.2 Å	Known		Weight of heads on myosin	Known
	dM3o		Known		Radial position of head origin	1
M6	IM6i			1	Weight of contribution from backbone	1
	IM6o			1	Axial position of backbone contribution	1
	dM6i	~7.16 Å	Known		Axial size of backbone diffractor	1
	dM6o		Known		Bare zone length	1
	IML1			1	Ratio of heads in to heads out	1
Interference	L		Known		Interference distance L	Known
Total observations				5	**Parameters**	20–32
Active muscle					Assume resting parameters if possible	
					Weight of heads	Known
M3	IM3i			1	Shape of heads on myosin	Assume as relaxed
	IM3o			1	Population of heads on myosin	1
	dM3i	~145.7 Å	Known		Distribution of head array on actin	4[b]
	dM3o		Known		Shape of heads on actin	(7–13[b]) × 2
M6	IM6i			1	Relative axial position of head array on actin	1
	IM6o			1	Weight of heads on actin	1
	dM6i		Known		Axial position of contribution from backbone	Assume as relaxed
	dM6o		Known		Weight of contribution from backbone	Assume as relaxed
	IML1			1	Population of heads in each attached state	1
Interference	L				Distribution of head array on myosin	Assume random
Total observations				10	**Parameters**	22–34

[a]Note that, to define head shape, one can assume a particular head structure that needs to be oriented in space with a tilt, a slew, and a rotation around its long axis (three parameters), or one could define it as a lever arm on which there is a mobile head domain: three parameters for the lever arm and three more parameters for the motor domain. In relaxed muscle, each of the two heads needs separate parameters, giving either 6 or 12 parameters, in addition to a parameter defining the separation of the head origins. In active muscle, there will be at least two populations of actin attached heads, each requiring 3 or 6 parameters to define the head shape (6–12 in all).

[b]Finding head attachment sites on actin requires two search parameters for the head (axial and azimuthal ranges) and a target area size and offset on the actin (two parameters). The axial distribution of labeled actin sites has a major effect on the values of M3 and M6; there are no heads on actin spaced 145.7 Å apart (I, intensity; d, distance; "known" means that the parameter value has been obtained experimentally). The table assumes that parameters for resting muscle can be determined first, and some of these can be used to help model active muscle.

with enough counts even for the weaker reflections to be reliable and including as many reflections as are needed to achieve a defined modeling outcome. (2) Transform the diffraction pattern into reciprocal space. (3) Carefully strip the background from the peaks of interest. Good software packages for data stripping are FiberFix (Rajkumar et al., 2007) or FIT2D (Hammersley, 2016). (4) Apply the Lorentz correction to the observed intensities that allows for the geometrical reduction of intensity in any fiber diffraction pattern as the radius from the meridian increases (Fraser and MacRae, 1973, p. 53). This is because, in a cylindrically averaged diffraction pattern, off-meridional peaks are smeared out into circles centered on the fiber axis, and the circumferences of the circles increase in proportion to the radius from the meridian (call it R). The larger R is, the more spread out the intensity is along the circumference and the less is recorded when it is sampled as in a diffraction pattern (by the Ewald sphere; see Eakins et al., 2019). To get corrected relative intensities, all that is required here is to multiply the observed intensities by R to give intensities that can be compared with those from a model computation. (5) Assess and justify how many truly independent observations (O) are available. (6) When doing modeling, count the number of carefully chosen adjustable parameters (P) that are being used. (7) If P is more than O, then the modeling cannot be performed unambiguously. The best thing to do is to reduce the number of parameters to something that can be justified and then not to make extravagant claims about the simpler model. (8) Start from the simplest possible model (with the fewest adjustable parameters) and test it

objectively against the observations by a goodness-of-fit factor (R-factor). If P is less than O so that good modeling can proceed and it is desired to add an extra parameter, then inclusion of the extra parameter is only justified if the goodness-of-fit factor (R-factor) is substantially lower than the R-factor of the previous model without that parameter (see Hamilton, 1965). If the R-factor is not substantially different from before, then inclusion of the extra parameter is not justified by the data.

Finally, Table 1 lists the minimum number of parameters that would be needed to start to define the configurations of the motor domains and lever arms of myosin heads in resting and contracting muscles in a sensible way in 3-D. The model allows for two detached states and two actin-attached head states in active muscle. A minimum of 20 parameters is needed to start modeling data from relaxed muscle using fixed head shapes. To model the lever arm configuration properly, the number of parameters goes up to ∼32 or more for relaxed muscle, depending on the level of detail that is required. As discussed above, in active muscle, the axial distribution of the attached heads on actin is crucial in defining M3 and M6 intensities, as well as the head shape and the population factors, and this really adds to the number of parameters required to create a full model from the whole 2-D low-angle diffraction pattern. The key thing to remember is that there are no actin-attached heads in active vertebrate muscle that are 145.7 Å apart axially, even though they contribute to the observed M3 peaks at 145.7 Å. It is not enough to try to model active muscle by putting attached heads on a 145.7 Å axial repeat and modifying their shape to try to fit the meridional and other parts of the pattern. This ignores the many other important factors that are involved in defining the M3 intensity.

If it is just the meridional intensities that are being used, then the myosin head shapes could reduce to fixed axially projected profiles of, for example, the Rayment et al. (1993) rigor and Dominguez et al. (1998) prepowerstroke shapes, assuming a particular configuration of the head on actin, rather than defining the head shape fully in 3-D. This would reduce the number of parameters needed to define each head shape from 6 per head to 0, assuming particular side-on profiles for the heads. But there is still the problem of knowing which head shapes occur on which specific actin-binding sites. So, even if something such as MusLabel (Squire and Knupp, 2004) defines likely binding sites on actin, the head shapes occupying different sites are uncertain. Vertebrate skeletal muscle has an approximate repeat after ∼15 crowns; for active muscle, this is 15 × 145.7 Å = 5 × 437.1 Å = 2,185.5 Å. 145.7 Å is the M3 crown repeat in active muscle; 437.1 Å is the myosin filament axial repeat (three crowns) in active muscle. This long repeat is close to three times the actin filament pitch of ∼715 Å (3 × 715 Å = 2,145 Å). In a unit cell containing one myosin filament and one set of surrounding actin filaments within a 2,185.5 Å axial repeat, there would be 15 × 6 myosin heads available to label actin, and it would be necessary to know (1) how many of these heads label actin in active muscle, (2) what is the axial distribution of the labeling sites, (3) how many of the attached heads were like Rayment et al. (1993) and how many were like Dominguez et al. (1998), (4) which of these two structures occurred on which actin binding sites, (5) what is the configuration of heads not on actin, and (6) what is the contribution from the filament backbone. More complicated models with more cross-bridge populations and shapes will obviously increase the number of unknown parameters. In addition, if the experiments are to look at changes as a function of sarcomere length (e.g., Reconditi et al., 2014) or as a function of temperature (e.g., Caremani et al., 2019), then many of these parameters will change with each sarcomere length or each temperature, and, although there will be extra data to model, the list of unknown parameters will increase accordingly. Factors such as the increasing axial misalignment of the myosin filaments as the sarcomere length increases will also affect the M3 and other meridional intensities.

Table 1 also lists how many observations there are if the only peaks being studied are those at M3, M6, and ML1, and only the ML1 total intensity is involved. This comes to 10 if the patterns from relaxed and active muscle are considered, well below the number of parameters needed to do even a very simple analysis in a reliable way. Very much more of the diffraction pattern is needed to make sensible headway, especially if we want to find out what the lever arms of the myosin heads are actually doing.

Conclusions

Time-resolved x-ray diffraction is an important and powerful means of probing the physiology of different muscle states. It is incumbent on those recording and analyzing the observations that they give the reader a realistic assessment of how reliable their conclusions are. Using diffraction observations as a tool is relatively straightforward. But if it is necessary to carry out modeling, then we need to show the number of parameters in the model and the number of independent observations that are being fitted. Without this, the modeling conclusions cannot be taken as justified.

Acknowledgments

Henk L. Granzier served as editor.

The authors are indebted to Danielle Paul and Marston Bradshaw for generation of Fig. 3 and to Edward Morris for generation of Fig. 8, b–d.

J.M. Squire was associated with the fellowship grant to Danielle Paul from the British Heart Foundation (FS/14/18/3071).

The authors declare no competing financial interests.

Author contributions: J.M. Squire and C. Knupp carried out the analysis; J.M. Squire and C. Knupp wrote the paper.

Submitted: 30 September 2020
Revised: 23 December 2020
Accepted: 12 July 2021

References

AL-Khayat, H.A., and J.M. Squire. 2006. Refined structure of bony fish muscle myosin filaments from low-angle X-ray diffraction data. *J. Struct. Biol.* 155:218–229. https://doi.org/10.1016/j.jsb.2006.03.029

Al-Khayat, H.A., N. Yagi, and J.M. Squire. 1995. Structural changes in actin-tropomyosin during muscle regulation: computer modelling of low-

angle X-ray diffraction data. *J. Mol. Biol.* 252:611–632. https://doi.org/10.1006/jmbi.1995.0524

AL-Khayat, H.A., L. Hudson, M.K. Reedy, T.C. Irving, and J.M. Squire. 2003. Myosin head configuration in relaxed insect flight muscle: x-ray modeled resting cross-bridges in a pre-powerstroke state are poised for actin binding. *Biophys. J.* 85:1063–1079. https://doi.org/10.1016/S0006-3495(03)74545-7

AL-Khayat, H.A., E.P. Morris, R.W. Kensler, and J.M. Squire. 2008. Myosin filament 3D structure in mammalian cardiac muscle. *J. Struct. Biol.* 163:117–126. https://doi.org/10.1016/j.jsb.2008.03.011

AL-Khayat, H.A., R.W. Kensler, J.M. Squire, S.B. Marston, and E.P. Morris. 2013. Atomic model of the human cardiac muscle myosin filament. *Proc. Natl. Acad. Sci. USA.* 110:318–323. https://doi.org/10.1073/pnas.1212708110

Bagni, M.A., B. Colombini, H. Amenitsch, S. Bernstorff, C.C. Ashley, G. Rapp, and P.J. Griffiths. 2001. Frequency-dependent distortion of meridional intensity changes during sinusoidal length oscillations of activated skeletal muscle. *Biophys. J.* 80:2809–2822. https://doi.org/10.1016/S0006-3495(01)76248-0

Behrmann, E., M. Müller, P.A. Penczek, H.G. Mannherz, D.J. Manstein, and S. Raunser. 2012. Structure of the rigor actin-tropomyosin-myosin complex. *Cell.* 150:327–338. https://doi.org/10.1016/j.cell.2012.05.037

Bennett, P., R. Craig, R. Starr, and G. Offer. 1986. The ultrastructural location of C-protein, X-protein and H-protein in rabbit muscle. *J. Muscle Res. Cell Motil.* 7:550–567. https://doi.org/10.1007/BF01753571

Bordas, J., G.P. Diakun, F.G. Diaz, J.E. Harries, R.A. Lewis, J. Lowy, G.R. Mant, M.L. Martin-Fernandez, and E. Towns-Andrews. 1993. Two-dimensional time-resolved X-ray diffraction studies of live isometrically contracting frog sartorius muscle. *J. Muscle Res. Cell Motil.* 14:311–324. https://doi.org/10.1007/BF00123096

Brenner, B., M. Schoenberg, J.M. Chalovich, L.E. Greene, and E. Eisenberg. 1982. Evidence for cross-bridge attachment in relaxed muscle at low ionic strength. *Proc. Natl. Acad. Sci. USA.* 79:7288–7291. https://doi.org/10.1073/pnas.79.23.7288

Brunello, E., P. Bianco, G. Piazzesi, M. Linari, M. Reconditi, P. Panine, T. Narayanan, W.I. Helsby, M. Irving, and V. Lombardi. 2006. Structural changes in the myosin filament and cross-bridges during active force development in single intact frog muscle fibres: stiffness and X-ray diffraction measurements. *J. Physiol.* 577:971–984. https://doi.org/10.1113/jphysiol.2006.115394

Brynnel, A., Y. Hernandez, B. Kiss, J. Lindqvist, M. Adler, J. Kolb, R. van der Pijl, J. Gohlke, J. Strom, J. Smith, et al. 2018. Downsizing the molecular spring of the giant protein titin reveals that skeletal muscle titin determines passive stiffness and drives longitudinal hypertrophy. *eLife.* 7:e40532. https://doi.org/10.7554/eLife.40532

Caremani, M., E. Brunello, M. Linari, L. Fusi, T.C. Irving, D. Gore, G. Piazzesi, M. Irving, V. Lombardi, and M. Reconditi. 2019. Low temperature traps myosin motors of mammalian muscle in a refractory state that prevents activation. *J. Gen. Physiol.* 151:1272–1286. https://doi.org/10.1085/jgp.201912424

Chandrasekaran, R., and G. Stubbs. 2012. International Tables for Crystallography. Vol. F., Chapter 19.5, 583–592. https://it.iucr.org/Fb/https://doi.org/10.1107/97809553602060000871

Colombini, B., M.A. Bagni, G. Cecchi, and P.J. Griffiths. 2007. Effects of solution tonicity on crossbridge properties and myosin lever arm disposition in intact frog muscle fibres. *J. Physiol.* 578:337–346. https://doi.org/10.1113/jphysiol.2006.117770

Cooke, R., and K. Franks. 1980. All myosin heads form bonds with actin in rigor rabbit skeletal muscle. *Biochemistry.* 19:2265–2269. https://doi.org/10.1021/bi00551a042

Daneshparvar, N., D.W. Taylor, T.S. O'Leary, H. Rahmani, F. Abbasiyeganeh, M.J. Previs, and K.A. Taylor. 2020. CryoEM structure of *Drosophila* flight muscle thick filaments at 7 Å resolution. *Life Sci. Alliance.* 3:e202000823. https://doi.org/10.26508/lsa.202000823

Dobbie, I., M. Linari, G. Piazzesi, M. Reconditi, N. Koubassova, M.A. Ferenczi, V. Lombardi, and M. Irving. 1998. Elastic bending and active tilting of myosin heads during muscle contraction. *Nature.* 396:383–387. https://doi.org/10.1038/24647

Dominguez, R., Y. Freyzon, K.M. Trybus, and C. Cohen. 1998. Crystal structure of a vertebrate smooth muscle myosin motor domain and its complex with the essential light chain: visualization of the pre-power stroke state. *Cell.* 94:559–571. https://doi.org/10.1016/S0092-8674(00)81598-6

Eakins, F., C. Pinali, A. Gleeson, C. Knupp, and J.M. Squire. 2016. X-ray diffraction evidence for low force actin-attached and rigor-like cross-bridges in the contractile cycle. *Biology (Basel).* 5:41. https://doi.org/10.3390/biology5040041

Eakins, F., J.J. Harford, C. Knupp, M. Roessle, and J.M. Squire. 2018. Different myosin head conformations in bony fish muscles put into rigor at different sarcomere lengths. *Int. J. Mol. Sci.* 19:2091. https://doi.org/10.3390/ijms19072091

Eakins, F., C. Knupp, and J.M. Squire. 2019. Monitoring the myosin crossbridge cycle in contracting muscle: steps towards 'Muscle-the Movie'. *J. Muscle Res. Cell Motil.* 40:77–91. https://doi.org/10.1007/s10974-019-09543-9

Ferenczi, M.A., S.Y. Bershitsky, N. Koubassova, V. Siththanandan, W.I. Helsby, P. Panine, M. Roessle, T. Narayanan, and A.K. Tsaturyan. 2005. The "roll and lock" mechanism of force generation in muscle. *Structure.* 13:131–141. https://doi.org/10.1016/j.str.2004.11.007

Fraser, R.D.B., and T.P. MacRae. 1973. Conformation in Fibrous Proteins and Related Synthetic Polypeptides. Academic Press, New York, London.

Hamilton, W.C. 1965. Significance tests on the crystallographic R-factor. *Acta Crystallogr.* 18:502–510. https://doi.org/10.1107/S0365110X65001081

Hammersley, A.P. 2016. *FIT2D*: a multi-purpose data reduction, analysis and visualization program. *J. Appl. Cryst.* 49:646–652. https://doi.org/10.1107/S1600576716000455

Harford, J., and J. Squire. 1986. "Crystalline" myosin cross-bridge array in relaxed bony fish muscle. Low-angle x-ray diffraction from plaice fin muscle and its interpretation. *Biophys. J.* 50:145–155. https://doi.org/10.1016/S0006-3495(86)83447-6

Harford, J.J., and J.M. Squire. 1992. Evidence for structurally different attached states of myosin cross-bridges on actin during contraction of fish muscle. *Biophys. J.* 63:387–396. https://doi.org/10.1016/S0006-3495(92)81613-2

Harford, J., and J. Squire. 1997. Time-resolved diffraction studies of muscle using synchrotron radiation. *Rep. Prog. Phys.* 60:1723–1787. https://doi.org/10.1088/0034-4885/60/12/005

Harford, J., P. Luther, and J. Squire. 1994. Equatorial A-band and I-band X-ray diffraction from relaxed and active fish muscle. Further details of myosin crossbridge behaviour. *J. Mol. Biol.* 239:500–512. https://doi.org/10.1006/jmbi.1994.1391

Hartt, J.E., and R.A. Mendelson. 1980. X-ray scattering of F-actin and myosin subfragment-1 complex. *Fed. Proc. Fed. Am. Soc. Exp. Biol.* 39:1728.

Haselgrove, J.C. 1973. X-ray evidence for a conformational change in the actin-containing filaments of vertebrate striated muscle. *Cold Spring Harb. Symp. Quant. Biol.* 37:341–352. https://doi.org/10.1101/SQB.1973.037.01.044

Haselgrove, J.C. 1975. X-ray evidence for conformational changes in the myosin filaments of vertebrate striated muscle. *J. Mol. Biol.* 92:113–143. https://doi.org/10.1016/0022-2836(75)90094-7

Haselgrove, J.C., and H.E. Huxley. 1973. X-ray evidence for radial cross-bridge movement and for the sliding filament model in actively contracting skeletal muscle. *J. Mol. Biol.* 77:549–568. https://doi.org/10.1016/0022-2836(73)90222-2

Holmes, K.C., and D.M. Blow. 1965. The use of x-ray diffraction in the study of protein and nucleic acid structure. *Methods Biochem. Anal.* 13:113–239. https://doi.org/10.1002/9780470110317.ch4

Holmes, K.C., D. Popp, W. Gebhard, and W. Kabsch. 1990. Atomic model of the actin filament. *Nature.* 347:44–49. https://doi.org/10.1038/347044a0

Hoskins, B.K., C.C. Ashley, G. Rapp, and P.J. Griffiths. 2001. Time-resolved X-ray diffraction by skinned skeletal muscle fibers during activation and shortening. *Biophys. J.* 80:398–414. https://doi.org/10.1016/S0006-3495(01)76023-7

Houdusse, A., and H.L. Sweeney. 2016. How myosin generates force on actin filaments. *Trends Biochem. Sci.* 41:989–997. https://doi.org/10.1016/j.tibs.2016.09.006

Hu, Z., D.W. Taylor, M.K. Reedy, R.J. Edwards, and K.A. Taylor. 2016. Structure of myosin filaments from relaxed *Lethocerus* flight muscle by cryo-EM at 6 Å resolution. *Sci. Adv.* 2:e1600058. https://doi.org/10.1126/sciadv.1600058

Hudson, L., J.J. Harford, R.C. Denny, and J.M. Squire. 1997. Myosin head configuration in relaxed fish muscle: resting state myosin heads must swing axially by up to 150 A or turn upside down to reach rigor. *J. Mol. Biol.* 273:440–455. https://doi.org/10.1006/jmbi.1997.1321

Huxley, H.E. 1953. X-ray analysis and the problem of muscle. *Proc. R. Soc. Lond. B Biol. Sci.* 141:59–62. https://doi.org/10.1098/rspb.1953.0017

Huxley, H.E. 1973. Structural changes in actin- and myosin-containing filaments during contraction. *Cold Spring Harb. Symp. Quant. Biol.* 37:361–376. https://doi.org/10.1101/SQB.1973.037.01.046

Huxley, H.E., and W. Brown. 1967. The low-angle x-ray diagram of vertebrate striated muscle and its behaviour during contraction and rigor. *J. Mol. Biol.* 30:383–434. https://doi.org/10.1016/S0022-2836(67)80046-9

Huxley, H.E., and M. Kress. 1985. Crossbridge behaviour during muscle contraction. *J. Muscle Res. Cell Motil.* 6:153–161. https://doi.org/10.1007/BF00713057

Huxley, H.E., A. Stewart, H. Sosa, and T. Irving. 1994. X-ray diffraction measurements of the extensibility of actin and myosin filaments in contracting muscle. *Biophys. J.* 67:2411–2421. https://doi.org/10.1016/S0006-3495(94)80728-3

Huxley, H., M. Reconditi, A. Stewart, and T. Irving. 2006a. X-ray interference studies of crossbridge action in muscle contraction: evidence from quick releases. *J. Mol. Biol.* 363:743–761. https://doi.org/10.1016/j.jmb.2006.08.075

Huxley, H., M. Reconditi, A. Stewart, and T. Irving. 2006b. X-ray interference studies of crossbridge action in muscle contraction: evidence from muscles during steady shortening. *J. Mol. Biol.* 363:762–772. https://doi.org/10.1016/j.jmb.2006.08.055

Irving, M., G. Piazzesi, L. Lucii, Y.B. Sun, J.J. Harford, I.M. Dobbie, M.A. Ferenczi, M. Reconditi, and V. Lombardi. 2000. Conformation of the myosin motor during force generation in skeletal muscle. *Nat. Struct. Biol.* 7:482–485. https://doi.org/10.1038/75890

Kabsch, W., H.G. Mannherz, D. Suck, E.F. Pai, and K.C. Holmes. 1990. Atomic structure of the actin:DNase I complex. *Nature.* 347:37–44. https://doi.org/10.1038/347037a0

Kiss, B., E.-J. Lee, W. Ma, F.W. Li, P. Tonino, S.M. Mijailovich, T.C. Irving, and H.L. Granzier. 2018. Nebulin stiffens the thin filament and augments cross-bridge interaction in skeletal muscle. *Proc. Natl. Acad. Sci. USA.* 115:10369–10374. https://doi.org/10.1073/pnas.1804726115

Kiss, B., J. Gohlke, P. Tonino, Z. Hourani, J. Kolb, J. Strom, O. Alekhina, J.E. Smith III, C. Ottenheijm, C. Gregorio, and H. Granzier. 2020. Nebulin and Lmod2 are critical for specifying thin-filament length in skeletal muscle. *Sci. Adv.* 6:eabc1992. https://doi.org/10.1126/sciadv.abc1992

Knupp, C., and J.M. Squire. 2019. Myosin cross-bridge behaviour in contracting muscle—the T_1 curve of Huxley and Simmons (1971) revisited. *Int. J. Mol. Sci.* 20:4892. https://doi.org/10.3390/ijms20194892

Knupp, C., G. Offer, K.W. Ranatunga, and J.M. Squire. 2009. Probing muscle myosin motor action: x-ray (m3 and m6) interference measurements report motor domain not lever arm movement. *J. Mol. Biol.* 390:168–181. https://doi.org/10.1016/j.jmb.2009.04.047

Knupp, C., E. Morris, and J.M. Squire. 2019. The interacting head motif structure does not explain the X-ray diffraction patterns in relaxed vertebrate (bony fish) skeletal muscle and insect (*Lethocerus*) flight muscle. *Biology (Basel).* 8:67. https://doi.org/10.3390/biology8030067

Lee, K.H., G. Sulbarán, S. Yang, J.Y. Mun, L. Alamo, A. Pinto, O. Sato, M. Ikebe, X. Liu, E.D. Korn, et al. 2018. Interacting-heads motif has been conserved as a mechanism of myosin II inhibition since before the origin of animals. *Proc. Natl. Acad. Sci. USA.* 115:E1991–E2000. https://doi.org/10.1073/pnas.1715247115

Linari, M., G. Piazzesi, I. Dobbie, N. Koubassova, M. Reconditi, T. Narayanan, O. Diat, M. Irving, and V. Lombardi. 2000. Interference fine structure and sarcomere length dependence of the axial x-ray pattern from active single muscle fibers. *Proc. Natl. Acad. Sci. USA.* 97:7226–7231. https://doi.org/10.1073/pnas.97.13.7226

Linari, M., E. Brunello, M. Reconditi, Y.B. Sun, P. Panine, T. Narayanan, G. Piazzesi, V. Lombardi, and M. Irving. 2005. The structural basis of the increase in isometric force production with temperature in frog skeletal muscle. *J. Physiol.* 567:459–469. https://doi.org/10.1113/jphysiol.2005.089672

Lombardi, V., G. Piazzesi, M. Reconditi, M. Linari, L. Lucii, A. Stewart, Y.B. Sun, P. Boesecke, T. Narayanan, T. Irving, and M. Irving. 2004. X-ray diffraction studies of the contractile mechanism in single muscle fibres. *Philos. Trans. R. Soc. Lond. B Biol. Sci.* 359:1883–1893. https://doi.org/10.1098/rstb.2004.1557

Lorenz, M., D. Popp, and K.C. Holmes. 1993. Refinement of the F-actin model against X-ray fiber diffraction data by the use of a directed mutation algorithm. *J. Mol. Biol.* 234:826–836. https://doi.org/10.1006/jmbi.1993.1628

Lovell, S.J., P.J. Knight, and W.F. Harrington. 1981. Fraction of myosin heads bound to thin filaments in rigor fibrils from insect flight and vertebrate muscles. *Nature.* 293:664–666. https://doi.org/10.1038/293664a0

Luther, P.K., and J.M. Squire. 1980. Three-dimensional structure of the vertebrate muscle A-band. II. The myosin filament superlattice. *J. Mol. Biol.* 141:409–439. https://doi.org/10.1016/0022-2836(80)90254-5

Luther, P.K., and J.M. Squire. 2014. The intriguing dual lattices of the Myosin filaments in vertebrate striated muscles: evolution and advantage. *Biology (Basel).* 3:846–865. https://doi.org/10.3390/biology3040846

Luther, P.K., H. Winkler, K. Taylor, M.E. Zoghbi, R. Craig, R. Padrón, J.M. Squire, and J. Liu. 2011. Direct visualization of myosin-binding protein C bridging myosin and actin filaments in intact muscle. *Proc. Natl. Acad. Sci. USA.* 108:11423–11428. https://doi.org/10.1073/pnas.1103216108

Lymn, R.W. 1978. Myosin subfragment-1 attachment to actin. Expected effect on equatorial reflections. *Biophys. J.* 21:93–98. https://doi.org/10.1016/S0006-3495(78)85510-6

Lymn, R.W., and E.W. Taylor. 1971. Mechanism of adenosine triphosphate hydrolysis by actomyosin. *Biochemistry.* 10:4617–4624. https://doi.org/10.1021/bi00801a004

Ma, W., H. Gong, B. Kiss, E.-J. Lee, H. Granzier, and T. Irving. 2018. Thick-filament extensibility in intact skeletal muscle. *Biophys. J.* 115:1580–1588. https://doi.org/10.1016/j.bpj.2018.08.038

Ma, W., K.H. Lee, S. Yang, T.C. Irving, and R. Craig. 2019. Lattice arrangement of myosin filaments correlates with fiber type in rat skeletal muscle. *J. Gen. Physiol.* 151:1404–1412. https://doi.org/10.1085/jgp.201912460

Martin-Fernandez, M.L., J. Bordas, G. Diakun, J. Harries, J. Lowy, G.R. Mant, A. Svensson, and E. Towns-Andrews. 1994. Time-resolved X-ray diffraction studies of myosin head movements in live frog sartorius muscle during isometric and isotonic contractions. *J. Muscle Res. Cell Motil.* 15:319–348. https://doi.org/10.1007/BF00123484

McNamara, J.W., A. Li, C.G. Dos Remedios, and R. Cooke. 2015. The role of super-relaxed myosin in skeletal and cardiac muscle. *Biophys. Rev.* 7:5–14. https://doi.org/10.1007/s12551-014-0151-5

Nelson, S.R., A. Li, S. Beck-Previs, G.G. Kennedy, and D.M. Warshaw. 2020. Imaging ATP consumption in resting skeletal muscle: one molecule at a time. *Biophys. J.* 119:1050–1055. https://doi.org/10.1016/j.bpj.2020.07.036

Offer, G., C. Moos, and R. Starr. 1973. A new protein of the thick filaments of vertebrate skeletal myofibrils. Extractions, purification and characterization. *J. Mol. Biol.* 74:653–676. https://doi.org/10.1016/0022-2836(73)90055-7

Padrón, R., W. Ma, S. Duno-Miranda, N. Koubassova, K.H. Lee, A. Pinto, L. Alamo, P. Bolaños, A. Tsaturyan, T. Irving, and R. Craig. 2020. The myosin interacting-heads motif present in live tarantula muscle explains tetanic and posttetanic phosphorylation mechanisms. *Proc. Natl. Acad. Sci. USA.* 117:11865–11874. https://doi.org/10.1073/pnas.1921312117

Parry, D.A.D., and J.M. Squire. 1973. Structural role of tropomyosin in muscle regulation: analysis of the x-ray diffraction patterns from relaxed and contracting muscles. *J. Mol. Biol.* 75:33–55. https://doi.org/10.1016/0022-2836(73)90527-5

Paul, D.M., J.M. Squire, and E.P. Morris. 2017. Relaxed and active thin filament structures; a new structural basis for the regulatory mechanism. *J. Struct. Biol.* 197:365–371. https://doi.org/10.1016/j.jsb.2017.01.004

Perutz, M.F. 1949. X-ray studies of crystalline proteins. *Research.* 2:52–61.

Perz-Edwards, R.J., T.C. Irving, B.A. Baumann, D. Gore, D.C. Hutchinson, U. Kržič, R.L. Porter, A.B. Ward, and M.K. Reedy. 2011. X-ray diffraction evidence for myosin-troponin connections and tropomyosin movement during stretch activation of insect flight muscle. *Proc. Natl. Acad. Sci. USA.* 108:120–125. https://doi.org/10.1073/pnas.1014599107

Piazzesi, G., M. Reconditi, M. Linari, L. Lucii, Y.B. Sun, T. Narayanan, P. Boesecke, V. Lombardi, and M. Irving. 2002. Mechanism of force generation by myosin heads in skeletal muscle. *Nature.* 415:659–662. https://doi.org/10.1038/415659a

Piazzesi, G., M. Reconditi, M. Linari, L. Lucii, P. Bianco, E. Brunello, V. Decostre, A. Stewart, D.B. Gore, T.C. Irving, et al. 2007. Skeletal muscle performance determined by modulation of number of myosin motors rather than motor force or stroke size. *Cell.* 131:784–795. https://doi.org/10.1016/j.cell.2007.09.045

Rajkumar, G., H.A. Al-Khayat, F. Eakins, C. Knupp, and J.M. Squire. 2007. The CCP13 FibreFix program suite: semi-automated analysis of diffraction patterns from non-crystalline materials. *J. Appl. Cryst.* 40:178–184. https://doi.org/10.1107/S0021889806048643

Rayment, I., W.R. Rypniewski, K. Schmidt-Bäse, R. Smith, D.R. Tomchick, M.M. Benning, D.A. Winkelmann, G. Wesenberg, and H.M. Holden. 1993. Three-dimensional structure of myosin subfragment-1: a molecular motor. *Science.* 261:50–58. https://doi.org/10.1126/science.8316857

Reconditi, M., N. Koubassova, M. Linari, I. Dobbie, T. Narayanan, O. Diat, G. Piazzesi, V. Lombardi, and M. Irving. 2003. The conformation of myosin head domains in rigor muscle determined by X-ray interference. *Biophys. J.* 85:1098–1110. https://doi.org/10.1016/S0006-3495(03)74547-0

Reconditi, M., M. Linari, L. Lucii, A. Stewart, Y.B. Sun, P. Boesecke, T. Narayanan, R.F. Fischetti, T. Irving, G. Piazzesi, et al. 2004. The myosin motor in muscle generates a smaller and slower working stroke at higher load. *Nature.* 428:578–581. https://doi.org/10.1038/nature02380

Reconditi, M., M. Linari, L. Lucii, A. Stewart, Y.B. Sun, T. Narayanan, T. Irving, G. Piazzesi, M. Irving, and V. Lombardi. 2005. Structure-function

relation of the myosin motor in striated muscle. *Ann. N. Y. Acad. Sci.* 1047:232–247. https://doi.org/10.1196/annals.1341.021

Reconditi, M., E. Brunello, L. Fusi, M. Linari, M.F. Martinez, V. Lombardi, M. Irving, and G. Piazzesi. 2014. Sarcomere-length dependence of myosin filament structure in skeletal muscle fibres of the frog. *J. Physiol.* 592: 1119–1137. https://doi.org/10.1113/jphysiol.2013.267849

Reedy, M.K. 1968. Ultrastructure of insect flight muscle. I. Screw sense and structural grouping in the rigor cross-bridge lattice. *J. Mol. Biol.* 31: 155–176. https://doi.org/10.1016/0022-2836(68)90437-3

Rome, E., G. Offer, and F.A. Pepe. 1973a. X-ray diffraction of muscle labelled with antibody to C-protein. *Nat. New Biol.* 244:152–154. https://doi.org/10.1038/newbio244152a0

Rome, E.M., T. Hirabayashi, and S.V. Perry. 1973b. X-ray diffraction of muscle labelled with antibody to troponin-C. *Nat. New Biol.* 244:154–155. https://doi.org/10.1038/newbio244154a0

Sjöström, M., and J.M. Squire. 1977. Fine structure of the A-band in cryo-sections. The structure of the A-band of human skeletal muscle fibres from ultra-thin cryo-sections negatively stained. *J. Mol. Biol.* 109:49–68.

Squire, J.M. 1972. General model of myosin filament structure. II. Myosin filaments and cross-bridge interactions in vertebrate striated and insect flight muscles. *J. Mol. Biol.* 72:125–138. https://doi.org/10.1016/0022-2836(72)90074-5

Squire, J.M. 1981. The Structural Basis of Muscular Contraction. Plenum Publishing Co., New York. https://doi.org/10.1007/978-1-4613-3183-4

Squire, J.M. 2000. Fibre and muscle diffraction. *In* Structure and Dynamics of Biomolecules. E. Fanchon, E. Geissler, L.-L. Hodeau, J.-R. Regnard, and P. Timmins, editors. Oxford University Press, Oxford, UK. 272–301.

Squire, J. 2019. Special issue: The actin-myosin interaction in muscle: background and overview. *Int. J. Mol. Sci.* 20:5715. https://doi.org/10.3390/ijms20225715

Squire, J.M., and C. Knupp. 2004. MusLABEL: a program to model striated muscle A-band lattices, to explore crossbridge interaction geometries and to simulate muscle diffraction patterns. *J. Muscle Res. Cell Motil.* 25: 423–438. https://doi.org/10.1007/s10974-004-3147-0

Squire, J.M., and C. Knupp. 2005. X-ray diffraction studies of muscle and the crossbridge cycle. *Adv. Protein Chem.* 71:195–255. https://doi.org/10.1016/S0065-3233(04)71006-2

Squire, J.M., and C. Knupp. 2017. Studies of muscle contraction using x-ray diffraction. *In* Muscle Contraction and Cell Motility: Fundamentals and Developments. H. Sugi, editor. Pan Stanford Publishing, Singapore. 35–73.

Squire, J.M., and E.P. Morris. 1998. A new look at thin filament regulation in vertebrate skeletal muscle. *FASEB J.* 12:761–771. https://doi.org/10.1096/fasebj.12.10.761

Squire, J.M., J.J. Harford, A.C. Edman, and M. Sjöström. 1982. Fine structure of the A-band in cryo-sections. III. Crossbridge distribution and the axial structure of the human C-zone. *J. Mol. Biol.* 155:467–494. https://doi.org/10.1016/0022-2836(82)90482-X

Squire, J.M., H.A. Al-Khayat, and N. Yagi. 1993. Muscle thin-filament structure and regulation: actin sub-domain movements and the tropomyosin shift modelled from low-angle X-ray diffraction. J. Chem. Soc. Faraday Trans. 89:2717–2726.

Squire, J.M., P.K. Luther, and C. Knupp. 2003. Structural evidence for the interaction of C-protein (MyBP-C) with actin and sequence identification of a possible actin-binding domain. *J. Mol. Biol.* 331:713–724. https://doi.org/10.1016/S0022-2836(03)00781-2

Squire, J.M., D.M. Paul, and E.P. Morris. 2017. Myosin and actin filaments in muscle: structures and interactions. *In Fibrous Proteins: Structures and Mechanisms. Subcellular Biochemistry*. Vol. 82. D. Parry and J. Squire, editors. Springer, Cham, Switzerland. 319–371. https://doi.org/10.1007/978-3-319-49674-0_11

Sweeney, H.L., A. Houdusse, and J. Robert-Paganin. 2020. Myosin Structures. *Adv. Exp. Med. Biol.* 1239:7–19. https://doi.org/10.1007/978-3-030-38062-5_2

Tolkatchev, D., D. Elnatan, L. Nogara, T. Ly, N. Naber, K. Haak, R. Meech, R. Cooke, and A.S. Kostyukova. 2018. Piperine, an alkaloid inhibiting the super-relaxed state of myosin, binds to the myosin regulatory light chain. *Arch. Biochem. Biophys.* 659:75–84. https://doi.org/10.1016/j.abb.2018.09.027

Tsaturyan, A.K., S.Y. Bershitsky, R. Burns, Z.H. He, and M.A. Ferenczi. 1999. Structural responses to the photolytic release of ATP in frog muscle fibres, observed by time-resolved X-ray diffraction. *J. Physiol.* 520: 681–696. https://doi.org/10.1111/j.1469-7793.1999.00681.x

Vainshtein, B.K. 1966. Diffraction of X-Rays by Chain Molecules. Elsevier, Amsterdam, London, New York.

Vibert, P., R. Craig, and W. Lehman. 1997. Steric-model for activation of muscle thin filaments. *J. Mol. Biol.* 266:8–14. https://doi.org/10.1006/jmbi.1996.0800

von der Ecken, J., S.M. Heissler, S. Pathan-Chhatbar, D.J. Manstein, and S. Raunser. 2016. Cryo-EM structure of a human cytoplasmic actomyosin complex at near-atomic resolution. *Nature.* 534:724–728. https://doi.org/10.1038/nature18295

Wakabayashi, K., Y. Sugimoto, H. Tanaka, Y. Ueno, Y. Takezawa, and Y. Amemiya. 1994. X-ray diffraction evidence for the extensibility of actin and myosin filaments during muscle contraction. *Biophys. J.* 67: 2422–2435. https://doi.org/10.1016/S0006-3495(94)80729-5

Wendt, T., D. Taylor, T. Messier, K.M. Trybus, and K.A. Taylor. 1999. Visualization of head-head interactions in the inhibited state of smooth muscle myosin. *J. Cell Biol.* 147:1385–1390. https://doi.org/10.1083/jcb.147.7.1385

Wlodawer, A., W. Minor, Z. Dauter, and M. Jaskolski. 2008. Protein crystallography for non-crystallographers, or how to get the best (but not more) from published macromolecular structures. *FEBS J.* 275:1–21. https://doi.org/10.1111/j.1742-4658.2007.06178.x

Woodhead, J.L., F.-Q. Zhao, R. Craig, E.H. Egelman, L. Alamo, and R. Padrón. 2005. Atomic model of a myosin filament in the relaxed state. *Nature.* 436:1195–1199. https://doi.org/10.1038/nature03920

Yamada, Y., K. Namba, and T. Fujii. 2020. Cardiac muscle thin filament structures reveal calcium regulatory mechanism. *Nat. Commun.* 11:153. https://doi.org/10.1038/s41467-019-14008-1

Yu, L.C., and B. Brenner. 1989. Structures of actomyosin crossbridges in relaxed and rigor muscle fibers. *Biophys. J.* 55:441–453. https://doi.org/10.1016/S0006-3495(89)82838-3

Zoghbi, M.E., J.L. Woodhead, R.L. Moss, and R. Craig. 2008. Three-dimensional structure of vertebrate cardiac muscle myosin filaments. *Proc. Natl. Acad. Sci. USA.* 105:2386–2390. https://doi.org/10.1073/pnas.0708912105